Inorganic Chemistry
Cite This: Inorg. Chem. 2019, 58, 4907−4920
Article
pubs.acs.org/IC

High-Frequency and -Field EPR (HFEPR) Investigation of a Pseudotetrahedral Cr^{IV} Siloxide Complex and Computational Studies of Related $Cr^{IV}L_4$ Systems

Lukas Bucinsky,[†] Martin Breza,[†] Michal Malček,[†] David C. Powers,[‡] Seung Jun Hwang,[§] J. Krzystek,[∥] Daniel G. Nocera,[§] and Joshua Telser*[,⊥]

[†]Institute of Physical Chemistry and Chemical Physics, Faculty of Chemical and Food Technology, Slovak University of Technology, Radlinského 9, SK-81237 Bratislava, Slovakia

[‡]Department of Chemistry, Texas A&M University, College Station, Texas 77843, United States

[§]Department of Chemistry and Chemical Biology, Harvard University, 12 Oxford Street, Cambridge, Massachusetts 02138, United States

[∥]National High Magnetic Field Laboratory, Florida State University, Tallahassee, Florida 32310, United States

[⊥]Department of Biological, Physical and Health Sciences, Roosevelt University, Chicago, Illinois 60605, United States

Supporting Information

ABSTRACT: Chromium species are the active sites in a variety of heterogeneous catalysts, such as the Phillips catalyst, which is composed of Cr ions supported by SiO_2 and is used to produce polyethylene. Among the catalytically relevant oxidation states of chromium is Cr^{IV}. Families of neutral, homoleptic, four-coordinate complexes, CrL_4, with a variety of monoanionic, monodentate ligands, such as L = alkyls, aryls, amides, ketimides ($R_2C = N^-$), alkoxides, and siloxides, are available and can provide information regarding Cr sites in heterogeneous materials. For example, the previously reported siloxide, $Cr(DTBMS)_4$, where DTBMS = $^-OSiMe^tBu_2$ (di-*tert*-butylmethylsiloxide), may be considered a molecular analogue of Cr^{IV} supported by SiO_2. Such CrL_4 complexes can have either a singlet ($S = 0$) or triplet ($S = 1$) spin ground state, and the spin state preferences of such complexes are not fully understood. A truly tetrahedral d^2 $S = 1$ complex would exhibit no zero-field splitting (zfs), and the zfs is indeed small and observable by X-band EPR for several CrR_4 and $Cr(OR)_4$ complexes. In contrast, $Cr(DTBMS)_4$ has zfs beyond the range amenable to X-band EPR so that high-frequency and high-field EPR (HFEPR) is appropriate. HFEPR of $Cr(DTBMS)_4$ in the solid state shows the presence of three very similar triplet species with the major component having $D = +0.556$ cm^{-1}. Classical ligand-field theory (LFT) and quantum chemical theory (QCT), including ab initio methods, use EPR and electronic absorption spectra to give a complete picture of the electronic structure of $Cr(DTBMS)_4$, and other complexes of formula $Cr(ER_n)_4$, E = C, $n = 3$; E = N, $n = 2$; E = O, $n = 1$; E = F, $n = 0$. Computations show the importance of ligand steric bulk and of π-bonding in controlling the subtleties of electronic structure of CrL_4 species. These electronic structure results, including zfs, which is a measure of excited state accessibility, for both triplet and singlet excited states, might be related to the catalytic activity of paramagnetic Cr species.

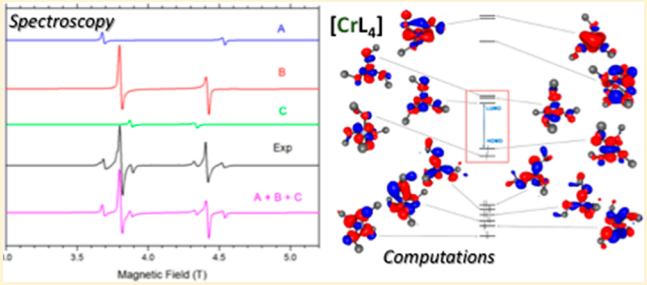

INTRODUCTION

The Phillips catalyst, based on silica-supported chromium, is used commercially to produce millions of tons of high-density polyethylene (HDPE) annually.[1−5] The mechanism for this heterogeneous catalyst is still not fully understood and, indeed, has been the source of some controversy in the literature.[6−8] Thus, insight into the nature of simple, molecular complexes of Cr in various oxidation states and with catalytically relevant ligands is of fundamental importance.[3] In particular, chromium alkyls are important as models for species involved in homogeneous catalytic reactions of saturated and unsaturated hydrocarbons,[9−11] and chromium alkoxides and siloxides have been investigated as models of heterogeneous, oxide-supported, chromium catalysts.[1−4,12,13]

Among the various chromium complexes that can serve as models for catalytically relevant species are $[Cr^{IV}(ER_n)_4]$ (E = C, N, O) complexes, which are of interest for several reasons. Among the many oxidation states available to chromium, Cr^{IV} ($3d^2$) is relatively uncommon, lacking the traditional (d block) coordination chemistry of Cr^{II} and Cr^{III}, but also lacking the p block-like stability/chemistry of Cr^{VI}. Homoleptic CrL_4

Received: December 17, 2018
Published: March 25, 2019

DOI: 10.1021/acs.inorgchem.8b03512
Inorg. Chem. 2019, 58, 4907−4920

complexes can exhibit either diamagnetic (spin singlet, $S = 0$) or paramagnetic (spin triplet, $S = 1$) ground states. The importance of multiple spin ground states and the accessibility of the corresponding excited states of different spin (e.g., ground $S = 1$, excited $S = 2$, or vice versa, for $d^{4,6}$; ground $S = 1$, excited $S = 0$, or vice versa, for $d^{2,8}$) has been shown to be important in catalytic activity.[14,15]

Homoleptic complexes of chromium(IV), CrL_4, where L = alkyl, amide, and alkoxide ligands that feature carbon, nitrogen, and oxygen donor atoms, respectively, were intensively studied beginning in the 1970s by the groups of Wilkinson,[16−19] Chisholm and Bradley,[20,21] and others.[9,22−25] Homoleptic tetraarylchromium(IV) complexes have been studied much more recently,[26,27] as have several heteroleptic tetraalkoxidochromium(IV) complexes, reported by Groysman, Villagrán, and Nocera.[28] Nocera and Marshak reported an isolable homoleptic tetrasiloxidochromium(IV) complex, $[Cr(OR)_4]$, $RO^- = {}^tBu_2MeSiO^-$ (DTBMS[29]), in 2013.[30] Ketimide ligands (i.e., ${}^tBu_2C{=}N^-$) have also been demonstrated to support homoleptic Cr^{IV} complexes.[31] CrL_4 complexes with ketimide ligands display singlet ground states,[31] but most others are triplets.

In a series of homoleptic complexes, one can use the metal ion as a reporter to understand quantitatively the nature of the ligand as was done historically in the spectrochemical series of M^{II} and M^{III} ions in particular.[32,33] A siloxide (R_3SiO^-) such as in $Cr(DTBMS)_4$ is of particular interest compared to an alkoxide (R_3CO^-) because the former has been suggested to participate in more ionic bonding with transition metal ions than the latter.[34]

As part of our interest in the electronic structure of *n*d complexes in high formal oxidation states,[35−38] and in the application of high-frequency and -field electron paramagnetic resonance (HFEPR) spectroscopy to 3d complexes in less common oxidation states,[39,40] we have combined a comprehensive computational study of the electronic structure of homoleptic tetracoordinate complexes of Cr^{IV} with HFEPR studies on one member of the series, $Cr(DTBMS)_4$. Here, we examine alkyl-substituted group 14−16 donors of the types R_3C^-, R_2N^-, RO^-, and, for completeness, CrF_4.[41−45] CrF_4 is not an isolable complex, but it does exist in rare gas matrices.[46] However, it is useful as a benchmark for a truly tetrahedral CrL_4 species, absent steric effects of the ligands and with cylindrical π interactions from them. The series of CrL_4 species of interest, given more specifically as $Cr(ER_n)_4$, E = C, N, O, F, $n = 3, 2, 1, 0$, is shown in Scheme 1, which also roughly describes the σ- and π donor properties of each ligand type.

Despite their triplet ground states, many CrL_4 (L = R, OR) complexes exhibit EPR spectra at conventional frequencies and fields (i.e., X-band: $\nu \approx 9$ GHz, $B_0 \approx 300$ mT),[16,17,21,24,25] as is the case for many organic triplets,[47,48] as a result of a zero-field splitting (zfs, given by the axial parameter, D) that is of small magnitude relative to the microwave energy quantum, $|D| < h\upsilon$. In contrast, the D value for $Cr(DTBMS)_4$ is roughly twice the magnitude of the X-band microwave quantum, making use of correspondingly larger frequencies and resonant magnetic fields imperative. We find that the Cr^{IV} amido complexes may have similar, or even larger, zfs, which was the cause of their EPR "silence" at X-band,[20] in contrast to the alkyl and alkoxido complexes. It is possible that zfs parameters, which are a measure of excited state accessibility, may be relevant among the multitude of oxidation and spin states available to Cr in supported catalysts,[1,4,5] as has been shown in other catalysts.[14,15,49]

Scheme 1. Overview of $CrL_4 = Cr(ER_n)_4$ Complexes, E = C, N, O, F; $n = 3, 2, 1, 0$

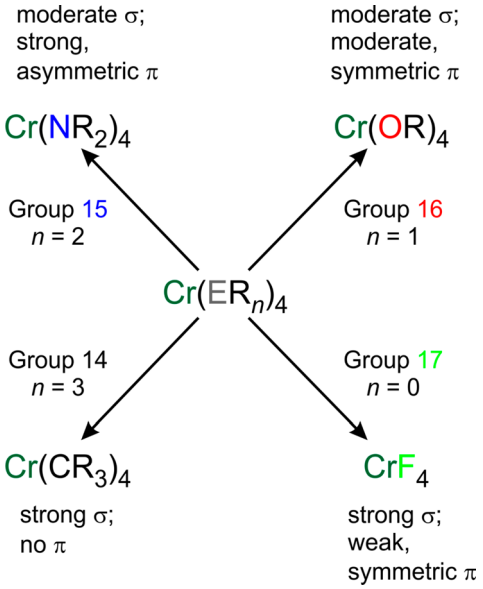

EXPERIMENTAL SECTION

Synthesis and Spectroscopy. $Cr(DTBMS)_4$ was prepared according to literature methods.[30] For HFEPR experiments, crystalline $Cr(DTBMS)_4$ was ground in an agate mortar and pestle in an Ar-filled glovebag and loaded into a Fisher vial sample holder. Upon grinding, the dark purple-brown crystals turned into a lighter purple-brown powder. Alternatively, the sample was dissolved in degassed toluene in the same glovebag and the purple-brown solution transferred to a Teflon container. HFEPR experiments were performed using the previously described spectrometer,[50] which was modified with a Virginia Diodes (Charlottesville, VA) source operating at 13 ± 1 GHz and generating frequencies between 48 and 336 GHz by a cascade of multipliers, at temperatures from liquid helium to ambient.

HFEPR spectra were simulated using the program SPIN (by A. Ozarowski), which employs a standard spin Hamiltonian for spin triplets:[48]

$$\mathcal{H} = \beta_e B\mathbf{g}\hat{S} + D\left(\hat{S}_z^{\,2} - \frac{1}{3}S(S+1)\right) + E(\hat{S}_x^{\,2} - \hat{S}_y^{\,2}) \quad (1)$$

Computational Details. Ligand-field theory (LFT) calculations were performed using the Ligfield program,[51] and the locally written programs DDN and DDNFIT, the latter of which allows fitting of LFT parameters to experimental d−d electronic absorption bands. These programs all use the full d^2 basis set. Free-ion values for the spin−orbit coupling (SOC) parameter, ζ, and Racah interelectronic repulsion parameters, B and C, were taken from those reported by Brorson, Bendix, and co-workers.[52,53]

Quantum Chemical Calculations. Geometry optimizations were performed using the Gaussian G09 program suite[54] employing the B3LYP/6-311G* level of theory.[55−61] The initial geometry for $Cr(DTBMS)_4$ optimization was based on the reported crystal structure.[30] The structure of $Cr(DTBMS)_4$ was also used as a starting point for $Cr(OSiMe_3)_4$ and $Cr(CH_2SiMe_3)_4$ following appropriate substituent truncations and replacement of −O− by $-CH_2-$ in the latter case. For $Cr({}^tBu)_4$ and $Cr(O{}^tBu)_4$, the reported structures of $Cr(cHx)_4$ (cHx = cyclohexyl[19]) and of $Cr(O{}^tBu)(OCMe{}^tBu_2)_3$[28] were used as initial structures for geometry optimization after the appropriate substituent modifications. The available crystal structure of $Cr(OCH{}^tBu_2)_4$[18] was used as an initial geometry for optimization

DOI: 10.1021/acs.inorgchem.8b03512
Inorg. Chem. 2019, 58, 4907−4920

of this complex as well as for optimization of $Cr(N(Me)(CH^tBu_2))_4$ following replacement of −O− by $-N(CH_3)-$. The complexes $Cr(OMe)_4$ and $Cr(NMe_2)_4$ were generated with a further structure truncation and visualization using Moldraw software.[62] The stability of all optimized structures in singlet and triplet ground states was evaluated by vibrational analysis. Stable structures obtained by closed-shell singlet state geometry optimizations were used for subsequent "broken symmetry" (BS) geometry reoptimizations using an unrestricted open-shell formalism. The BS method has been widely used, in particular by Neese and co-workers,[63−67] to investigate transition metal complexes with "noninnocent" ligands having (potential) radical character, such as semiquinones[63,64,66] and thiosemicarbazones.[65,67]

The energy difference between singlet (E_S) and triplet (E_T) state is evaluated as given in eq 2:

$$E_S = E_T = \frac{(E_{BS} - E_{uT})}{(1 - 0.5\langle S^2\rangle_{BS})} \quad (2)$$

where E_{uT} is an unrestricted open-shell energy of the triplet state, and E_{BS} and $\langle S^2\rangle_{BS}$ are the energy and spin expectation values of the broken symmetry (BS) singlet state, respectively.[63,68]

The zfs parameters[69] and **g** tensors[70,71] were evaluated using the ORCA software package (version 4.0.1.2).[72,73] The UBLYP[55,56]/TZVP[74] zfs parameters were calculated with the quasirestricted orbital (QRO) method.[69] The complete active space self-consistent field (CASSCF)[69,75−77] results were based on an active space of 2 electrons in 5 orbitals (2,5), to account for the d electrons of chromium, using 10 state averaged triplet states (15 singlet states were determined in the CI expansion of the state averaged triplet solutions).

The D and E contributions shown are based upon the state averaged formalism, using 10 triplet and 15 singlet states. The spin−spin coupling (SSC) contribution to the CASSCF(2,5) D and E parameters was evaluated from a minimal multireference configuration interaction calculation (denoted here as $MRCI_{MIN}$)[69,75] in the state averaged active space of 2 electrons in 5 orbitals. Dynamic electron correlation effects were accounted for via the N-Electron Valence State Perturbation Theory to second order (NEVPT2)[78−81] in the case of smaller sized systems.

The electronic structure of the complexes under study has been explored at the BLYP, B3LYP, and state averaged CASSCF levels of theory. Nevertheless, the DFT level of theory is taken as the reference, treating dynamic electron correlation effects via the DFT correlation potential. Two functionals (B3LYP and BLYP), which treat the exchange contributions in a slightly different manner having an impact on the spin state preference, have been chosen. Although the CASSCF/NEVPT2 level of theory is the more rigorous one (compared to DFT), the treatment of d orbitals as active is capable of assessing the electronic configuration of the central atom in a manner well-suited for the evaluation of (HF)EPR parameters, rather than for the characterization of ligand-field interactions in the CASSCF wave function. The electronic structure at the DFT level of theory was elucidated via BLYP localized orbitals,[82] unrestricted natural orbitals (UNOs), and Mulliken population analysis of atomic d orbitals, as well as B3LYP Quantum Theory of Atoms in Molecules (QTAIM) analysis.[83] A brief description of the QTAIM analysis method with respect to electron density topology is given in Supporting Information, Section III.

QTAIM analysis at the B3LYP/6-311G* level of theory was performed in the AIMAll package[84] using the wave functions from the G09 wfn file. Localized BLYP/6-311G* orbitals (see Figures S8 and S9) and unrestricted natural orbitals, UNOs (see Figures 6, 7, and S10), were visualized in the IQmol software package.[85]

The program SHAPE was used to provide a measure as to the overall deviation of selected CrL_4 complexes, whether in crystallographic or optimized geometries, from ideal tetrahedral symmetry.[86,87]

RESULTS AND DISCUSSION

EPR Spectroscopy. Conventional (e.g., X-band) EPR is observable for spin triplets only if the zero-field splitting (zfs) is comparable, or preferably smaller, than the available microwave energy quantum ($|D| \leq h\upsilon$). This is the case for a number of CrL_4 complexes: where L = R = 1-norbornyl (Nor),[25] $CH_2CMe_nPh_{3-n}$ (n = 0−3);[16,17,24] L = Ar^{nCl} = pentachlorophenyl, 2,4,6-trichlorophenyl, and 2,6-dichlorophenyl;[26,27] and L = OR = O^{t}Bu anions.[21] In certain cases,[17] X-band EPR spectra exhibited a triplet pattern,[47,48] with resolved fine structure, so that zfs parameters could be directly extracted. A detailed discussion of conventional EPR spectra of ML_4 (M = d^2 ion) complexes is given in Supporting Information, Section I.

In contrast, $Cr(DTBMS)_4$ has substantial zfs (at X-band, $|D| > h\upsilon$) and is thus a case where HFEPR can be fruitfully employed. HFEPR has been applied to a number of octahedral d^8 complexes (chiefly of Ni^{II}),[88−92] but not to the corresponding electron/hole system of tetrahedral d^2, with the exception of an oxide material doped with Mn^V ions ($Ba_2In_{2-x}Mn_xO_{5+x}$).[93] The present study is thus the first application of HFEPR to a tetrahedral d^2 ion in a molecular system.

HFEPR spectra of $Cr(DTBMS)_4$ exhibited powder patterns characteristic for a triplet (S = 1) spin state at all frequencies and temperatures employed in this study. Such spectra consist of a single "half-field" turning point of $\Delta M_S = \pm 2$ transition (also called B_{min}) accompanied by the turning points of the allowed $\Delta M_S = \pm 1$ resonances at higher fields. We have observed only the perpendicular turning points, which is a frequent phenomenon because in a powder pattern the parallel features are much weaker and are easily lost in the noise. Figure 1 shows the spectra recorded at 10 K and five different frequencies.

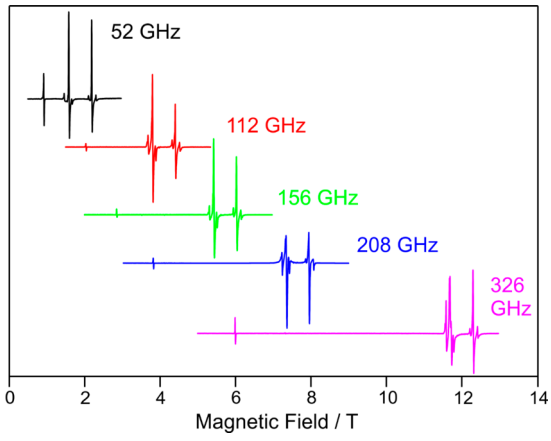

Figure 1. EPR spectra of $Cr(DTBMS)_4$ recorded at 10 K and at different frequencies (indicated on the plot).

The $\Delta M_S = \pm 1$ turning points are structured at all frequencies employed. This structure at multiple frequencies could be simulated only by assuming the presence of three different triplet species, which we name here A, B, and C, with species B being the dominant one. Each of the observed species possesses a unique set of spin Hamiltonian parameters representing an axial zfs tensor. The simulated combination of these three axial species at a single frequency is shown in Figure 2. The axial nature of zfs in $Cr(DTBMS)_4$ is

DOI: 10.1021/acs.inorgchem.8b03512
Inorg. Chem. 2019, 58, 4907−4920

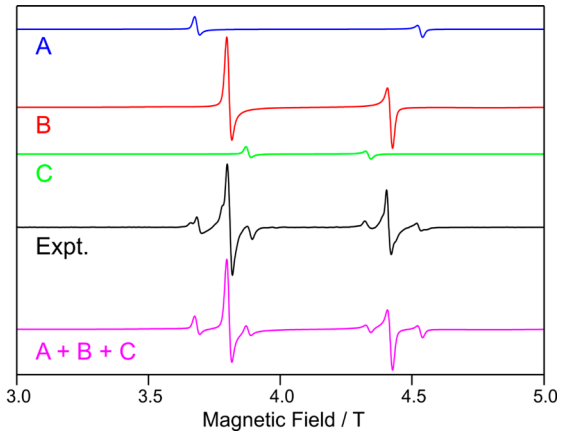

Figure 2. Experimental (black trace) and simulated (colored traces) HFEPR spectra (at 112 GHz) for $Cr(DTBMS)_4$ showing the experimental spectrum being composed of three species (A (blue), B (red; major component), and C (green)), with their sum in magenta. The simulation parameters are given in Table 1.

corroborated by the theoretical results (vide infra), and by the structure: crystallographic 2-fold and improper 4-fold (S_4) symmetry. Interestingly, a very similar situation, i.e., three different $S = 1$ species, each of them characterized by an axial zfs tensor, was found in a high-spin cobalt(I) system.[94]

In addition to the magnitude, the sign of zfs is also of interest. Figure 3 shows a spectrum at 10 K and 112 GHz

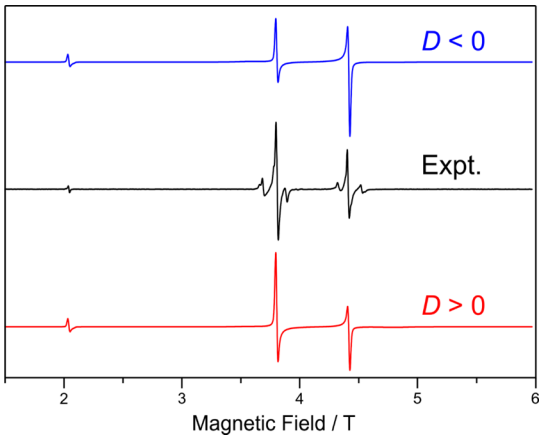

Figure 3. EPR spectrum of 1 at 10 K and 112 GHz (black trace) accompanied by simulations using spin Hamiltonian parameters for the dominant species (B) as in Table 1. Blue trace; negative D; red trace, positive D.

accompanied by simulations using spin Hamiltonian parameters for the major species B only. It is apparent that the axial zfs parameter D is positive for this species. Similar simulations were performed for the other two species, and the spin Hamiltonian parameters are collected in Table 1. In each case, $D > 0$, the significance of which will be discussed in the LFT section below.

HFEPR spectra obtained from low-temperature toluene solutions confirmed the order of magnitude of the zfs. Unfortunately, additional information could not be extracted from these spectra because instead of three discrete triplet states, as observed in the solid, the solution spectra showed a continuum of spin species characterized by D values contained between species A and C.

Table 1. Spin Hamiltonian Parameters for Three Spin Triplet Species Observed in Solid $Cr(DTBMS)_4$

species	D (cm^{-1})	$g_\perp$	$g_\parallel$ [a]	g_{avg} [b]
A	+0.757	1.930	1.8	1.89
B (majority)	+0.556	1.935	1.9	1.92
C	+0.416	1.935	1.9	1.92

[a]No parallel $\Delta M_S = \pm 1$ turning points were observed in the spectra. The $g_\parallel$ value was deducted so as to bring the B_{min} transition to the right field. [b]This value is provided for comparison with calculated values discussed below.

It should be noted that although there are multiple, similar spin triplet (i.e., Cr^{IV}) species present, there are *no* signals from other paramagnetic chromium spin states, such as Cr^{II} (spin quintet), Cr^{III} (spin quartet), or Cr^{V} (spin doublet). Similar heterogeneity was observed by Mowat et al. for the complexes CrR_4 (R = CH_2CMe_3, CH_2SiMe_3, and CH_2CMe_2Ph), even in frozen petroleum ether solution,[17] and by Ward et al. for $Cr(Nor)_4$ in frozen isooctane.[25] The resonances are visible at all temperatures examined, up to and including ambient temperature. There are many temperature-dependent spectral changes occurring between low and room temperature, particularly in the 50−150 K range, Figure 4. We have not

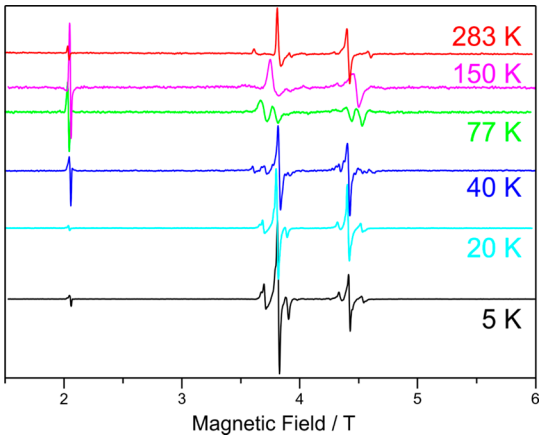

Figure 4. EPR spectra of $Cr(DTBMS)_4$ at 112 GHz and varying temperature (as indicated on the plot).

tried to interpret these features absent detailed XRD data at variable temperatures. We note again that similar temperature-dependent changes were observed by Mowat et al. in frozen solution for the tetraalkyl complexes listed above.[17] For example, the parallel (z) fine structure splitting (zfs) of $Cr(CH_2SiMe_3)_4$ ranged from 0.12 cm^{-1} (~130 mT) at 140 K to 0.15 cm^{-1} (~160 mT) at 125 K (~20% change), at which point two species developed, the larger of which reaches nearly 0.19 cm^{-1} (200 mT).[95]

Ligand-Field Theory (LFT). *Electronic Absorption Spectra.* As is the case for essentially all $3d^2$ ML_4 complexes,[96] all of the CrL_4 complexes of interest are very close to ideal tetrahedral symmetry as quantified by the continuous shape measures protocol as implemented by Alemany, Alvarez, and co-workers.[86,87] The results are summarized in Table S2 and confirm that T_d symmetry is a good approximation for the application of ligand-field theory (LFT). In T_d symmetry there are three spin-allowed transitions: $^3A_2$ ($e^2t_2^0$ in strong field notation) → $^3T_2$ ($e^1t_2^1$), $^3A_2$ → $^3T_1(F)$ ($e^1t_2^1$), and $^3A_2$ → $^3T_1(P)$ ($e^0t_2^2$).[17] The first of these is symmetry (dipole)

DOI: 10.1021/acs.inorgchem.8b03512
Inorg. Chem. 2019, 58, 4907−4920

Table 2. Electronic Absorption Bands of CrL_4 Complexes of Interest with All Energies in cm^{-1}

	band assignment in T_d symmetry from $^3A_2(F)$ ground state				crystal-field parameters[b]		
complex	$\rightarrow {}^3T_2(F)$	$\rightarrow {}^3T_1(F)$[a]	$\rightarrow {}^3T_1(P)$[a]	$\rightarrow$singlets	B	C	Dq
$Cr(Nor)_4$[c]	16 130	20 580	– (CT at 29 850, 34 010)	18 730, 18 080	410	1685	1613
$Cr(NEt_2)_4$[d]	13 700	–	– (CT at 25 000–50 000)	–	500	2055	1370
$Cr(O^tBu)_4$[e]	9100 (8700, 9500)	15 200	25 000 (CT at 37 000, 45 000)	–	816.4	3355	927.7
$Cr(DTBMS)_4$[f]	8070	12 500	– (CT at 36 000)	9600, 18 520	530.7	2040.8	807.0

[a]The free-ion parentage of these terms is very mixed, and the lower-energy term can in some cases have a higher ^3P parentage, while the higher-energy term correspondingly has a higher ^3F parentage, but we label all of these, respectively, as from ^3F and ^3P to correspond with the traditional Tanabe–Sugano diagram (see Figure 5 and Figure S1). [b]This model uses only tetrahedral crystal field splitting (Dq parameter) with Racah interelectronic repulsion parameters B and C (the latter not independently determined, but set at 4.11B, except for $Cr(DTBMS)_4$). Analysis using the AOM is given in SI (see Tables S3–S5). [c]Data taken from Abrahamson et al.[97] [d]Data taken from Basi et al.[20] Only one vis band was observed (at 730 nm). [e]Data taken from Alyea et al.[21] For the lowest-energy band, the center of gravity (9100) is used for crystal-field fitting, but two bands (given in parentheses) were observed, due to tetragonal distortion from tetrahedral symmetry. The table gives results of a consensus fit for all three bands, while the following parameter set matches the two higher-energy bands exactly but the lowest less well (see Table S3): Racah B = 794, C = 3260, Dq = 943. [f]Data taken from Marshak and Nocera.[30] An alternate analysis with an assumption as to the $^3A_2 \rightarrow {}^3T_1(P)$ transition is discussed in SI (see Table S3 and Figure S1).

forbidden in T_d symmetry (and might be well into the NIR region), and the last is a two-electron transition (and might be in the UV region), so oftentimes only a single d–d transition is observed.

The electronic absorption data for relevant CrL_4 complexes are summarized in Table 2, along with tetrahedral crystal-field parameters. Further discussion on these complexes is given in Supporting Information, section VI. Due to its dominant position in this study, we review here the electronic absorption data for $Cr(DTBMS)_4$, which exhibits an informative electronic absorption spectrum that was thoroughly analyzed by Marshak and Nocera.[30] There is a UV band at 278 nm, assigned to CT (its extinction coefficient is more than 4-fold that of the strongest vis band), and four vis–NIR features that were assigned to d–d transitions (in T_d symmetry), two spin-allowed and two spin-forbidden, as follows: 540 nm (18 520 cm^{-1}, ε = 140), assigned to $^3A_2(F) \rightarrow {}^1T_1(G)$; 800 nm (12 500 cm^{-1}, ε = 900), assigned to $^3A_2 \rightarrow {}^3T_1(F)$; 1042 nm (9600 cm^{-1}, sh), assigned to $^3A_2 \rightarrow {}^1E(D)$; and 1240 nm (8070 cm^{-1}, ε = 60), assigned to $^3A_2 \rightarrow {}^3T_2(F)$. Use of a general Tanabe–Sugano diagram yielded B = 530 cm^{-1} (only ~50% of the free-ion value[52]) and Dq = 794 cm^{-1}, which is less than that derived for $Cr(O^tBu)_4$ (see Table 2), but not unreasonable given the expected poorer donor ability of a siloxide relative to an alkoxide ion. We have reanalyzed the electronic absorption spectra for $Cr(DTBMS)_4$, first using a tetrahedral crystal field. The spin-allowed transitions at 800 and 1240 nm are fitted exactly with B = 530 cm^{-1} and Dq = 807 cm^{-1}, essentially identical to Marshak and Nocera.[30] It is then possible, by varying the Racah C parameter, to fit exactly the spin-forbidden transition at 540 nm (18 520 cm^{-1}; see Tables S3 and S4e). For illustration, particularly of the singlet excited states, an energy level diagram using these Racah parameters and a range of crystal-field spitting is shown in Figure 5.[98]

We next applied the angular overlap model (AOM)[99] to the geometry of $Cr(DTBMS)_4$ derived from crystallography. Without the need for π-bonding, it is possible to match the spin-allowed transitions exactly and come close to fitting the spin-forbidden ones. The resulting parameters are B = 486.6 cm^{-1}, ε_0 = 6294.4 cm^{-1}, i.e., slightly weaker π-bonding than in $Cr(O^tBu)_4$, as would be expected for the siloxide. The Racah B parameter is quite low, which is consistent with the analogous alkyl complexes (see Table 2). Inclusion of a small degree of π-

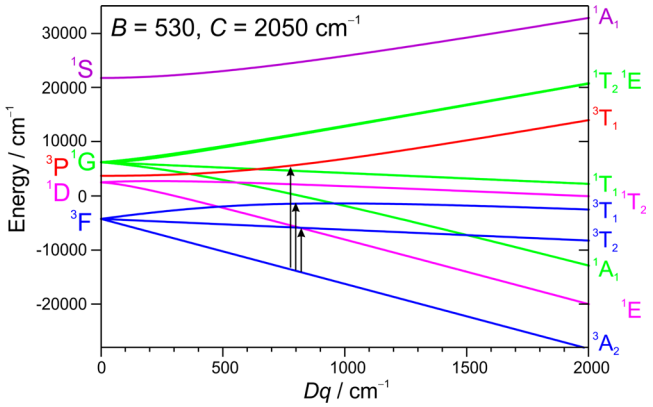

Figure 5. Energy level diagram for $Cr(DTBMS)_4$ generated using Racah parameters B = 530 cm^{-1}, C = 2050 cm^{-1}, and the tetrahedral crystal field splitting range as indicated on the abscissa. The three vertical arrows represent possible assignments using $Dq \approx$ 800 cm^{-1} of the three transitions observed at (left to right) 18 520 cm^{-1} (540 nm), 12 500 cm^{-1} (800 nm), and 8070 cm^{-1} (1240 nm).[30] Ligand-field energy levels corresponding to this Dq value are given in Table S4e.

bonding ($\varepsilon_{\pi\text{-c}}$ = 230.0 cm^{-1}) allows all of the spin-allowed and -forbidden bands to be matched exactly (see Table S3), with only modest changes in the other parameters. The resulting ligand-field energy levels, with free-ion parentage, are given in Table S4.

EPR Spectra and Spin Hamiltonian Parameters. Concerning the nearly tetrahedral complexes that yield conventional EPR spectra, there is a perturbation theory expression for the g value (as observed for the ΔM_S = 1 ("ordinary") transition):[21,100]

$$g = g_e\left[1 - \frac{4k^2\lambda_0}{10Dq}\right] = g_e\left[1 - \frac{4k\lambda'}{10Dq}\right] \quad (3)$$

where g_e is the free electron g value (2.0023), λ_0 is the multielectron spin–orbit coupling (SOC) constant ($\lambda_0 = \zeta/2S$; ζ = 319 cm^{-1} for free-ion Cr^{4+}),[53] k is the Stevens orbital reduction factor ($0 < k \leq 1$, which reduces SOC: $\lambda' = k\lambda_0$), and $10Dq$ is the tetrahedral ligand-field splitting.[101] Alyea et al. observed g = 1.962 for $Cr(O^tBu)_4$, which they attributed to $k \approx$ 0.6, indicating significant covalency.[102] For $Cr(Nor)_4$, 1.986 $\leq g \leq$ 1.990,[25] so use of $10Dq$ = 16 130 cm^{-1}, determined above,

DOI: 10.1021/acs.inorgchem.8b03512
Inorg. Chem. 2019, 58, 4907–4920

gives k = 0.424. These suggest higher covalency in the tetraalkyl versus tetraalkoxy complex. The remaining complex for which g values are available, and in this case well-determined by HFEPR, is $Cr(DTBMS)_4$. The above crystal-field analysis suggests that the tetrahedral splitting in this complex is roughly 8000 cm^{-1}, and the three species identified gave g_{avg} = 1.89 (A) or 1.92 (B (major species) and C; see Table 1). These values, respectively, yield k = 0.84 and 0.72, which are not as reduced from free-ion values as the Racah parameters used for the above LFT analysis of the electronic absorption spectrum of $Cr(O^tBu)_4$,[103,104] but still indicative of covalency.

Mowat et al. have also provided a perturbation theory expression for the D value in distorted tetrahedral complexes,[17] based on spin−orbit coupling (SOC) between the ground state and low-lying triplet and singlet excited states (eq 4):[105]

$$D = \zeta^2 \left\{ \begin{aligned} &+\frac{1}{\Delta E[^3E\{^3T_2(F)\}]} - \frac{1}{\Delta E[^3B_2\{^3T_2(F)\}]} \\ &-\frac{1}{\Delta E[^1E\{^1T_2(D)\}]} + \frac{1}{\Delta E[^1B_2\{^1T_2(D)\}]} + \frac{1}{\Delta E[^1B_2\{^1T_2(G)\}]} - \frac{1}{\Delta E[^1E\{^1T_2(G)\}]} \end{aligned} \right\} \quad (4)$$

The ΔE denominators represent the energy of the respective excited state above the $^3B_1(^3A_2(F))$ ground state. For truly tetrahedral symmetry, there is no splitting within the $^{3,1}T_2$(F, D, G) terms so the denominators of each T_2-derived pair become equal, canceling out so that D becomes zero. What is clear from eq 4 is that the sign of D depends on the relative energies of the two components of the split $^{3,1}T_2$(F, D, G) terms, with the $^3T_2(F)$-derived pair being by far dominant as it is much lower in energy than those from the two singlet terms (see Figure 5). The AOM used for $Cr(DTBMS)_4$, namely, the slightly distorted tetrahedron, indeed has ^3E ($^3T_2(F)$) lower in energy than $^3B_2(^3T_2(F))$ so the calculated D value is positive, as seen by HFEPR. The specific contributions of each excited state were determined by QCT (Supporting Information, Section V and Table S15), and are fully consistent with LFT.

Use of the AOM described above with inclusion of SOC then reproduces the zfs observed by HFEPR for $Cr(DTBMS)_4$ (see Table S5). The ζ value needed for this successful calculation is ∼60% of the free-ion value (i.e., $k \approx 0.6$), consistent with the above perturbation theory. Further application of the AOM is described in Supporting Information, Section V, wherein it is shown that very slight angular changes ($\Delta(\theta, \phi) < 1°$) can potentially lead to the differing zfs values of the several components seen by HFEPR.

Quantum Chemical Theory (QCT). We first address the energetically favored geometries and spin states, followed by a discussion of the EPR-derived spin Hamiltonian parameters and conclude with a brief comparison of the electronic structure of the CrL_4 complexes, particularly with respect to their ground state spin preferences.

Optimized Geometries. We have performed B3LYP/6-311G* geometry optimization of a wide range of neutral molecules of general structure CrL_4, where L = alkyl, amide, alkoxide, and siloxide, and B3LYP/6-311+G* geometry optimization of CrF_4, in both singlet and triplet ground states. The results of the geometry optimizations as reflected by the metrical parameters of the Cr inner coordination sphere, together with experimental data, where available, are summarized in Table S1. The results of the ground state B3LYP/6-311+G* energy calculations of singlets and triplets are summarized in Table S8 (additional comparisons of triplet versus singlet total BLYP, CASSCF, and NEVPT2 energies are given in Tables S10 and S11).

For both CrF_4, in agreement with previous work,[44] and the tetraalkyl complexes, the calculations show essentially tetrahedral geometry as expected for a cylindrical π donor in the former and pure σ donors in the latter complexes. Geometrical differences between the experimentally found triplet and putative singlet states are relatively minor. Steric effects clearly play a role as seen in the sole structurally characterized CrR_4 complex, $Cr(cHx)_4$,[19] which has bulkier R groups than the calculated complexes, which were chosen because of their relationship to spectroscopically characterized complexes. In the case of $Cr(CH_2SiMe_3)_4$, the tetraalkyl analogue of $Cr(OSiMe_3)_4$, itself the simplified variant of $Cr(DTBMS)_4$, one can infer some steric effects in the deviation of two of the C−Cr−C bond angles by roughly ±2° from ideal tetrahedral geometry.

In contrast, the amido and alkoxide/siloxide complexes show greater calculated distortions from tetrahedral geometry, with deviations of as much as roughly ±7° in certain cases. Interestingly, the triplet ground state calculations generally appear to be slightly more tetragonally distorted than the singlets, although such a distortion would be necessary to favor a singlet ground state (compression raising d_{z^2} relative to $d_{x^2-y^2}$). In no case, however, is the distortion very large, in contrast to the ketimide complex, $Cr(N{=}C^tBu_2)_4$, for which the large pair of N−Cr−N bond angles equals 136.8° (27.3° deviation from ideal T_d) and the complex indeed has a singlet ground state.[31] The π interactions in such tetrakisketimide complexes, $M(N{=}CR_2)_4$, in contrast to those of the unconjugated π donors studied here, are very significant,[31,38] and will be the subject of a separate computational study. As can be seen in Table 3, the calculated B3LYP/6-311G* energy difference between the singlet and triplet states is substantial; e.g., the reaction $^3[Cr(ER_n)_4](g) \rightarrow {}^1[Cr(ER_n)_4](g)$ (n = 3, 2, 1; R = Me) has $\Delta G_{298} \approx$ +163, +81, +41 kJ/mol, respectively, for E = C, O, N. This trend arises from an increase in π interactions as the pure σ donor alkyl, which is unable to effect anisotropy in the e orbitals, is replaced by the weak 2e (or even 4e) π donor alkoxide, with the amide being the strongest 2e π donor, increasing the energy of the d_{z^2} orbital via $\varepsilon_{\pi\text{-}c}$, as proposed to occur in $V(N{=}C^tBu_2)_4$.[38,106] The spin state preferences at the BLYP and CASSCF/NEVPT2 levels of theory are suggesting singlet state preference in the case of amido complexes,[107] while the triplet ground state is confirmed for the remaining classes of complexes (see Tables S10 and S11).[108]

Electronic Structures. We begin with the Quantum Theory of Atoms in Molecules (QTAIM) analysis. For simplicity, we

DOI: 10.1021/acs.inorgchem.8b03512
Inorg. Chem. 2019, 58, 4907−4920

Table 3. Singlet (S)−Triplet (T) Energy Separation Evaluated According to Equation 2 at B3LYP/6-311G* Level of Theory

compd	$(E_S - E_T)_{DFT}$ [kJ/mol]	$(G_S - G_T)_{298}$ [kJ/mol]
CrF_4[a]	328.7	335.2
	Alkyl Complexes	
$Cr(CH_2SiMe_3)_4$	134.9	152.0
Cr^tBu_4	149.7	163.4
	Amido Complexes	
$Cr(NMeCH^tBu_2)_4$	64.6	83.6
$Cr(N^tBu_2)_4$	–	–
$Cr(NMe_2)_4$	26.8	40.6
	Alkoxide Complexes	
$Cr(OCH^tBu_2)_4$	102.4	123.1
$Cr(O^tBu)_4$	89.2	75.3
$Cr(OMe)_4$	69.7	81.7
	Siloxide Complexes	
$Cr(OSiMe_3)_4$	103.0	128.1
$Cr(DTBMS)_4$	102.7	103.7

[a]6-311+G* basis set.

restrict discussion of our QTAIM B3LYP/6-311G* study to the most preferred spin states of these complexes (see Table 3). The QTAIM BCP analysis results are summarized in Tables S6 and S7. On the basis of ρ_{BCP} data, the bond strengths decrease in the sequence Cr−F > Cr−O > Cr−C as do the particular bond lengths (compare Tables S6 and S1, respectively). Excepting $Cr(NMeCH^tBu_2)_4$, the remaining Cr−N bond strengths are comparable with the Cr−O ones. The dative character of the bonds, as indicated by $\nabla^2\rho_{BCP}$ data, exhibit a similar trend: Cr−F > Cr−O > Cr−N > Cr−C. BCP ellipticities, ε_{BCP}, indicate pure σ-bonding only in CrF_4 and Cr^tBu_4. Nevertheless, low ε_{BCP}, high BCP electron densities, ρ_{BCP}, as well as the presence of π-bonding localized orbitals and the structure of UNOs (see Tables S9 and S13a, respectively) indicate symmetric π-bonding Cr−F interactions (analogous to a weak triple bond as in ethyne).

Very high ε_{BCP} values for amidos indicate π-bonding interactions (probably the interaction with a lone electron pair at N). Note that the continuous shape measures analysis shows that the deviation from ideal T_d symmetry is largest, albeit still very small, for the optimized tetraamido complexes (see Table S2). Relatively small values of the delocalization indices, DI, for the amido $Cr(NMeCH^tBu_2)_4$ compound are in agreement with ρ_{BCP} indicating weaker Cr−N bonding, while the $Cr(NMe_2)_4$ amido compound has comparable ρ_{BCP} and DI as in the alkoxides and siloxides, although the ε_{BCP} is considerably larger and Cr−O bonding with respect to their π-character (ε_{BCP} values) indicates that π interactions need not be stronger than the σ ones. The main point to mention with respect to the QTAIM bond characteristics compiled in Table S6 is that the bulkiness of the ligands (except alkyls) seems to

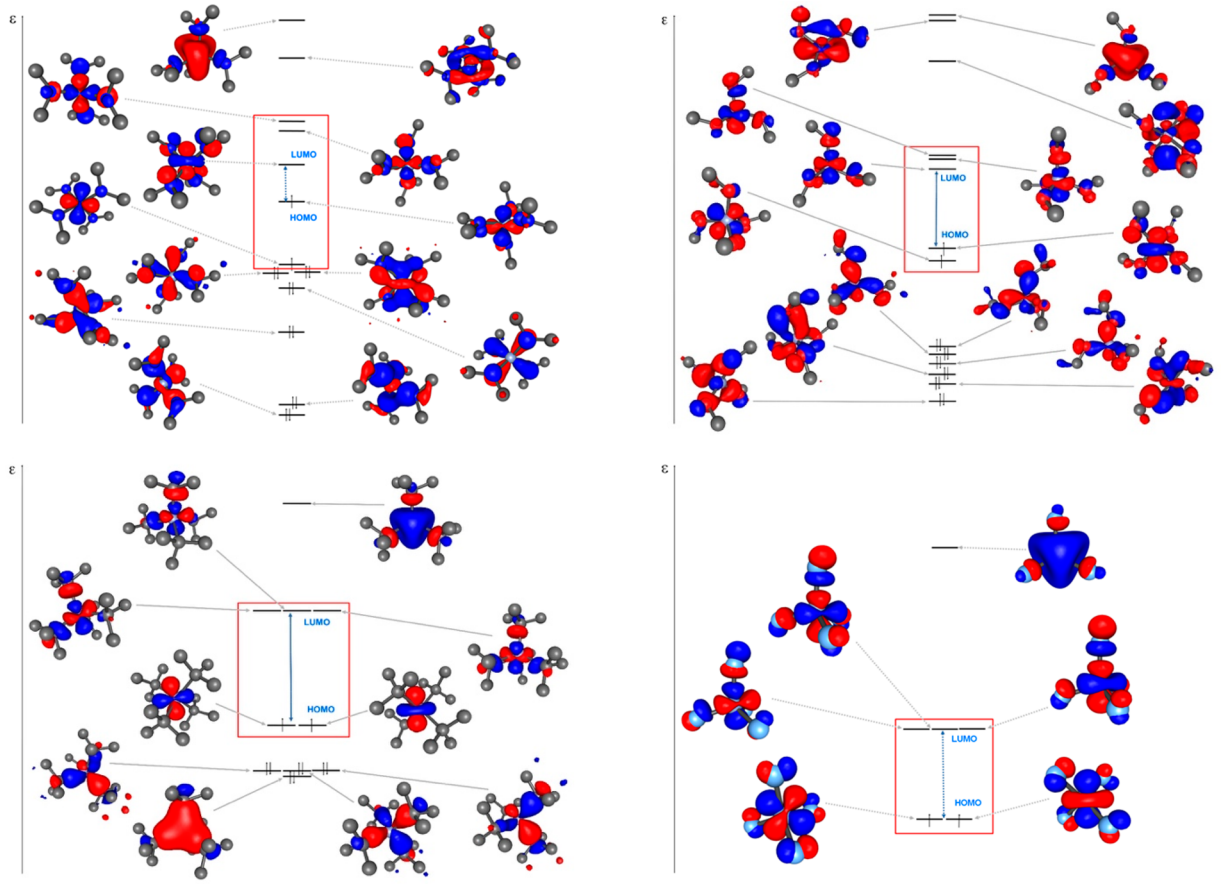

Figure 6. BLYP/6-311G* UNOs of essentially Cr(3d, 4s)−E(2s, 2p) hybridization for $Cr(ER_n)_4$ (R = Me, E = C, N, O, F; n = 3, 2, 1, 0) complexes. Lower left: Cr^tBu_4. Upper left: $Cr(NMe_2)_4$. Upper right: $Cr(OMe)_4$. Lower right: CrF_4. HOMO and LUMO orbitals have respective α eigenvalues (in hartree) of −0.1659 and −0.0737 (Cr^tBu_4); −0.1209 and −0.0561 (triplet ground state $Cr(NMe_2)_4$); −0.1439 and −0.0801 ($Cr(OMe)_4$); −0.2417 and −0.1692 (CrF_4). The red boxes highlight the orbitals with significant Cr 3d character.

DOI: 10.1021/acs.inorgchem.8b03512
Inorg. Chem. 2019, 58, 4907−4920

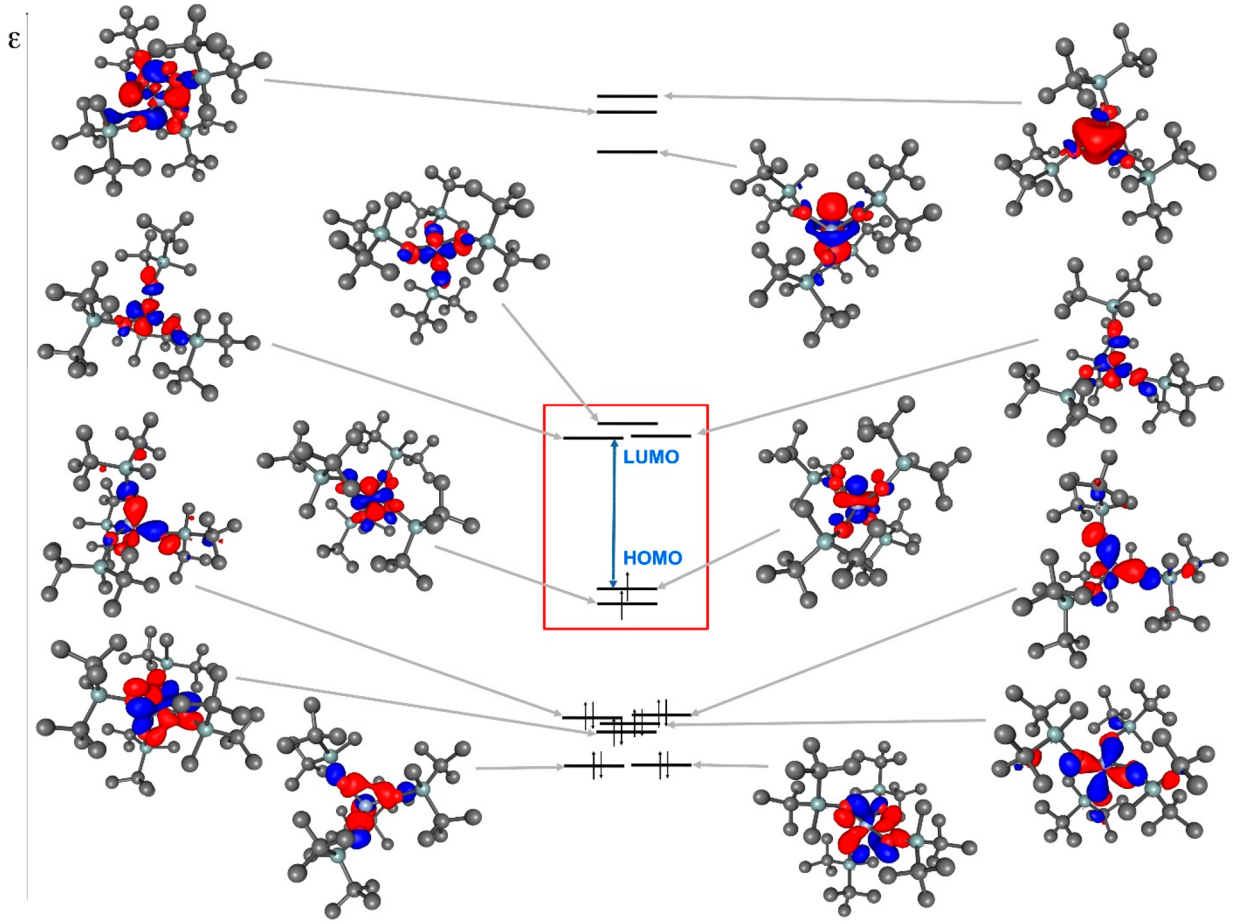

Figure 7. BLYP/6-311G* UNOs for $Cr(DTBMS)_4$ of essentially Cr(3d, 4s)−O(2s, 2p) hybridization. HOMO and LUMO orbitals have α eigenvalues of −0.1656 and −0.1092 hartree, respectively. The red box highlights the orbitals with significant Cr 3d character.

closely correlate with weakening of the dative Cr−L bonds. Results on the localized BLYP/6-311G* orbitals and Mulliken d orbital populations on the central Cr atom are compiled in Table S9, and the particular localized orbitals of Cr^tBu_4, $Cr(NMe_2)_4$, and $Cr(OMe)_4$ are shown in Figure S8. Populations of the BLYP/6-311G* localized orbitals agree qualitatively well with the QTAIM bond characteristics for the B3LYP/6-311G* electron density. In particular, the population of the localized orbitals has both of the largest π contributions in the case of amidos in comparison to alkoxides and siloxides. Still, the bonding populations on Cr in the localized orbitals representation (see Table S9) are overall nearly the same, and only the weight of the dative σ or π contributions changes.

Unrestricted Natural Orbitals (UNOs), calculated using the BLYP/6-311G* basis set, have been utilized to analyze the Cr−ER_n bonding interactions in a pictorial way. UNOs allow one to obtain a qualitative picture of the Cr−L bonding character and the orbital ordering using a relatively small number of orbitals. We present here UNO diagrams for the representative simplest systems of each $Cr(ER_n)_4$ type, R = Me; E = C, N, O, F; n = 3, 2, 1, 0 (Figure 6), with their relative position the same as in Scheme 1, plus the main complex of interest, $Cr(DTBMS)_4$ (Figure 7). The (Mulliken-like) compositions of UNOs shown in Figures 6 and 7 are compiled in Table S13. For Cr^tBu_4 (Figure 6, lower left), it is relatively easy to see that the highest occupied UNO corresponds to the degenerate $d_{x^2-y^2}$ (α) and d_{z^2} (α)orbitals. For $Cr(OMe)_4$ (Figure 6, upper right), the highest occupied UNO is clearly of a d_{z^2} (α)-like character. The simple structure of CrF_4 (Figure 6, lower right) does not allow us to show all the UNOs of the Cr−F interactions using the same energy scale as for the other such figures; see Table S13a for further details.

For $Cr(DTBMS)_4$, the first six lowest doubly occupied UNOs are σ and mixed σ/π bonding Cr−O orbitals (the lowest three have a Cr population below 20%; the other three slightly above 25%). The two open shells are essentially of 3d(Cr) character (around 81%). Above these in energy are three non-bonding orbitals of 3d(Cr) character (72%). Finally, there are three π- and σ-antibonding Cr−O orbitals (population on Cr atom around 50%). The situation is far more complex in the case of canonical Kohn−Sham orbitals (not shown), while the σ and π interactions are presented via localized orbitals in Figure S9.

Spin Hamiltonian Parameters. The calculated spin Hamiltonian parameters (zfs and g values) are compiled in Table 4. It can be seen that, in agreement with experiment,[17,24,25] the calculated zfs for the tetraalkyl complexes is very small in magnitude, with nearly isotropic g values slightly below g_e, also as expected and found experimentally. The complex with the β-Si (i.e., $Cr(CH_2SiMe_3)_4$) shows a slightly larger calculated zfs and deviation in g from g_e relative to that with only light atom ligands, which might be a consequence of the larger SOC for a 3p versus 2p atom.[109,110] For the amido compounds, the zfs is considerably affected by the coordination geometry. The large magnitude of the CASSCF D value is caused by the presence of a low-lying excited state which

DOI: 10.1021/acs.inorgchem.8b03512
Inorg. Chem. 2019, 58, 4907−4920

Table 4. Calculated Spin Hamiltonian (zfs and g Tensor) Parameters in the 6-311G* Basis Set[a]

compd	method	D (cm^{-1})	E (cm^{-1})	g_{xx}	g_{yy}	g_{zz}	g_{iso}
CrF_4	BLYP	−0.011	−0.003	1.977	1.977	1.977	1.977
	CASSCF	−0.016 (−0.019)	−0.004 (−0.005)	1.926	1.926	1.926	1.926
	NEVPT2	−0.022	−0.001	1.936	1.936	1.937	1.936
			Alkyl Complexes				
$Cr(Nor)_4$[b]	expt I−IV	0.027[a,I] 0.023[a,II] 0.013 [a,III] 0.012 [a,IV]	0.0041[a,I] 0.0027[a,II] 0.0032[a,III] 0.0029[a,IV]				(1.9905)[b]
$Cr(CH_2SiMe_3)_4$	BLYP	−0.058	−0.014	1.991	1.992	1.992	1.992
	CASSCF	+0.092 (+0.097)	+0.026 (+0.081)	1.950	1.951	1.952	1.951
Cr^tBu_4	BLYP	+0.001	0.000	1.993	1.993	1.993	1.993
	CASSCF	+0.005 (+0.005)	+0.001 (+0.001)	1.947	1.948	1.948	1.948
			Amido Complexes				
$Cr(NMeCH^tBu_2)_4$	BLYP	+1.459	+0.143	1.975	1.982	1.987	1.981
	CASSCF	−62.730 (−63.321)	−0.663 (−0.777)	1.191	1.862	1.882	1.645
	NEVPT2	−9.776	−0.420	1.802	1.953	1.963	1.906
$Cr(NMe_2)_4$	BLYP	−0.042	+0.000	1.985	1.987	1.987	1.987
	CASSCF	−0.935 (−0.992)	+0.002 (+0.002)	1.938	1.954	1.954	1.949
$Cr(NMe_2)_4$	BLYP	−1.827	−0.204	1.971	1.985	1.994	1.983
C_2 symm	CASSCF	−154.369 (−155.346)	−0.882 (−0.877)	0.625	1.604	1.619	1.283
	NEVPT2	−1.953	−0.356	1.820	1.953	1.973	1.915
			Alkoxide Complexes				
$Cr(OCH^tBu_2)_4$	BLYP	−0.564	0.000	1.968	1.978	1.978	1.975
	CASSCF	−2.045 (−2.087)	−0.001 (−0.001)	1.896	1.927	1.927	1.917
$Cr(O^tBu)_4$	BLYP	+0.868	0.000	1.974	1.974	1.984	1.977
	CASSCF	+1.772 (+1.780)	0.000 (0.000)	1.920	1.920	1.947	1.929
	expt[c]	<0.3					1.962
$Cr(OMe)_4$	BLYP	+1.249	+0.172	1.980	1.982	1.985	1.982
	CASSCF	+1.173 (+1.492)	+0.084 (+0.084)	1.931	1.935	1.952	1.939
	NEVPT2	+0.905	+0.046	1.943	1.948	1.961	1.951
			Siloxide Complexes				
$Cr(OSiMe_3)_4$	BLYP	0.352	0.000	1.972	1.972	1.976	1.974
	CASSCF	+0.789 (+0.804)	0.000 (0.000)	1.920	1.920	1.931	1.923
	NEVPT2	+0.748	0.000	1.929	1.929	1.941	1.933
$Cr(DTBMS)_4$	BLYP	+0.287	+0.028	1.972	1.972	1.975	1.973
expt geom	CASSCF	+0.704 (+0.719)	+0.072 (+0.080)	1.915	1.918	1.927	1.920
$Cr(DTBMS)_4$	BLYP	+0.098	+0.002	1.9702	1.9702	1.9721	1.9708
opt geom	CASSCF	+0.425	+0.006	1.9127	1.9128	1.9185	1.9146
	expt[d]	+0.556	0.0	1.935	1.935	1.9	1.92

[a]In parentheses are shown the results of the $MRCI_{MIN}$ calculations. Relevant experimental data are also given. [b]Taken from Ward et al.[25] Four conformations were identified (denoted I−IV) for $Cr(Nor)_4$ in frozen isooctane solution at 93 K, and the zfs parameters for each are given (no sign determination was possible, hence no sign is provided). The g value given is from a single crystal measurement at room temperature and thus does not directly correspond to the frozen solution data. [c]Taken from Alyea et al.[21] There was evidence for small magnitude zfs, but its value was not determined. The upper limit given is based on the X-band microwave quantum energy. [d]The experimental value for only species B (the major one) is given here; see Table 1 for the full data set.

becomes corrected by the NEVPT2 treatment.[111,112] In particular, the CASSCF and/or NEVPT2 calculations for $Cr(NMeCH^tBu_2)_4$ and a C_2 symmetry geometry of $Cr(NMe_2)_4$ are consistent with previous experimental results. Basi et al. measured the magnetic susceptibility of $Cr(NEt_2)_4$ over the temperature range 298−98 K and observed μ_{eff} = 2.87(1) between 98 and 223 K,[20] i.e., the spin-only value for S = 1. However, even if $|D|$ were as large as 10 cm^{-1}, μ_{eff} would be unchanged over this temperature range and not show a notable decrease until ∼10 K, reaching ∼2.06 at 4 K (for D > 0). These workers would have also had little chance of observing conventional EPR spectra from such triplet species with $|D| \gg h\upsilon$.[113] $Cr(O^tBu)_4$ does give an EPR signal near g = 2,[21] so the D values calculated here may be overestimated; however, it is possible that, with multiple conformations, there may be one that has a small magnitude for D. Finally, for $Cr(DTBMS)_4$, the only complex with non-negligible zfs for which the spin Hamiltonian parameters are well-determined, the calculations for the experimental geometry agree reasonably well with experiment.[114−116] The orientation of the calculated **D** tensor for $Cr(DTBMS)_4$ is shown in Figure 8 and clearly shows that the principal zfs axis coincides with the molecular S_4 axis, in agreement with LFT.

We also wished to probe computationally the effect that geometrical structure has on the zfs parameters, which is related to the heterogeneity seen in (HF)EPR for both tetraalkyl complexes with small magnitude zfs[24,25] and our siloxide complex with relatively larger zfs. This was done in two ways, the first being to take the two more sterically bulky alkoxides, $Cr(OCH^tBu_2)_4$ and $Cr(O^tBu)_4$, and "strip" each down to $Cr(OMe)_4$ (i.e., $^tBu_2$ to H_2 and Me_3 to H_3, respectively), without changing their optimized geometries. Alkoxides rather than alkyls were chosen because the latter have such small magnitude zfs in the first place. This

DOI: 10.1021/acs.inorgchem.8b03512
Inorg. Chem. 2019, 58, 4907−4920

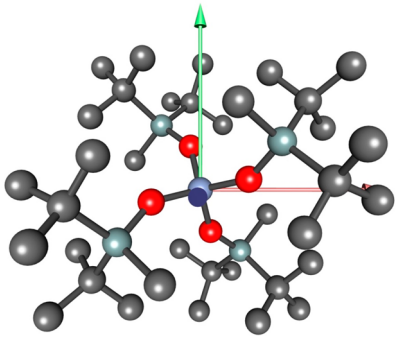

Figure 8. Structure of $Cr(DTBMS)_4$ (H atoms omitted; Cr, blue; C, gray; O, red; Si, light gray) with superimposed zfs (**D**) tensor directions: *z*-axis, light green; *x*-axis, dark blue (out of page); *y*-axis (pink). The Euler angles of this tensor with respect to the molecular frame (deg) are −13.1629 (α), 90.0041 (β), −179.9995 (γ).

truncation has little effect on the calculated zfs parameters for the "new" $Cr(OMe)_4$ species, which thus remain different in their zfs parameters from those of the original $Cr(OMe)_4$, see Table S14. Thus, geometry has a greater effect than the electronic effects of different R groups. The second approach was a more "brute force" one, namely, to take $Cr(OMe)_4$ in ideal tetrahedral geometry and distort it systematically to each of the C_{2v}, C_{3v}, and D_{2d} geometries by, respectively, shortening/elongating two (C_{2v}) or one (C_{3v}) Cr−O bond distance(s) or changing a pair of opposite O−Cr−O bond angles (D_{2d}), each changing in a stepwise fashion with the zfs calculated for each structure. For comparison, the same process is applied to CrF_4.[117] The results are summarized in Figures S11 and S12 and clearly show the extreme sensitivity of the *D* value.[118] As also seen using the AOM (see Supporting Information, Section II), angular (i.e., D_{2d}) distortions lead to huge changes in *D*, but still with the sign tracking with compression (positive) or elongation (negative). In the former case, *D* becomes very large (e.g., ∼10 cm^{-1} for ∼140° ≤ ∠O−Cr−O ≤ ∼160°), until it decreases in the hypothetical square planar (D_{4h}) case. The effects of bond length changes are much harder to generalize, but, qualitatively, show that the sign and magnitude of *D* can fluctuate widely, especially in the trigonal distortion case.

Electronic Absorption Spectra. Calculated electronic absorption spectra of selected CrL_4 complexes in both singlet and triplet ground states are discussed and presented in Supporting Information, Section VI (Table S12 and Figures S13−S28). The CASSCF(2,5) d−d transitions are usually red-shifted (up to 400 nm in the case of $Cr(DTBMS)_4$ compared to NEVPT2 and TD-DFT results). All of the complexes show calculated electronic transitions in the UV region (≥∼30 000 cm^{-1}) with substantial oscillator strengths (f > 0.1) that are due to CT transitions and are consistent with experiment. Calculated vibrational spectra are also presented in tandem with the electronic spectra (Figures S13−S28).

Relevance to Catalysis. In contrast, for example, to the studies in parallel by the Copéret[2,6,8,13] and Scott[1,4,5,7,11] groups, we do not claim to provide direct insight into the mechanism of Cr-based heterogeneous, or even homogeneous, catalysis. Nevertheless, there are several qualitative lessons that can be drawn from our and from previous experimental work and from the present extensive computational studies on $Cr(ER_n)_4$ species. The first is that even relatively simple tetraalkyl complexes (E = C, n = 3), while unequivocally exhibiting spin triplet ground states, can show substantial conformational flexibility and that there can be electronic or steric effects from heavier atoms (i.e., Si) that are not directly coordinated. The optimized geometry of $Cr(CH_2SiMe_3)_4$ has shorter Cr−C bond lengths than Cr^tBu_4 (see Table S1). Moreover, the axial distortion that can lead to either compression along the S_4 axis, which manifests in positive *D*, or elongation, which manifests in negative *D*, can lead to effectively more singlet-like (M_S = 0 lowest energy) behavior in the former case, or still triplet-like behavior in the latter (M_S = ±1 lowest), which could affect reactivity. This point is obviously more relevant in the E = N and O cases where the magnitude of *D* can be much larger. The $Cr(NR_2)_4$ species are especially interesting, with the strong and anisotropic π donor ability of the amido ligands. Our computational studies show, as experimental data are scant but intriguing, that $Cr(NR_2)_4$ might have very relatively low-lying singlet excited states, which could make Cr^{IV} amidos potentially useful for homogeneous catalysis as postulated for other, chiefly Fe-containing, systems.[14,15,49] Sadly, there is less analogy to heterogeneous catalysts than for the alkoxide/siloxide systems. Our results on $Cr(OR)_4$ further support the conformational flexibility of this type of complex, which even oxide-supported Cr^{IV} might exhibit. This flexibility and the zfs effect mentioned above, arising from modest, but still significant, π-donation by the oxido ligands, are clearly greater for siloxides than alkoxides; e.g., see BCP ellipticities in Table S6. Although the singlet excited states in $Cr(OR)_4$ are less accessible than in $Cr(NR_2)_4$, they may still play a role, especially in higher-energy catalytic intermediates.

CONCLUSIONS

A comprehensive computational investigation, supported by EPR spectra of selected examples, of the electronic structure of homoleptic, tetracoordinate chromium(IV) complexes has been performed. These CrL_4 complexes comprise a variety of donor atoms in their simplest forms, C as alkyl (L = R_3C^-), N as amide (L = R_2N^-), and O as alkoxide (L = RO^-), with L = F included for completeness, although no thermally stable molecular complex of formula CrF_4 exists, only a low-temperature, matrix isolated species.[44,46] These complexes have spin triplet ground states with very small magnitude zfs so that conventional (e.g., X-band) EPR was sufficient to observe readily interpretable spectra, as reported many years ago. In contrast, the Cr^{IV} siloxido complex, $Cr(DTBMS)_4$, is not amenable to conventional EPR field/frequency conditions. We have therefore performed HFEPR studies on this complex, which to our knowledge is the first such application to a molecular complex of Cr^{IV}, and found it to have $D \approx +0.5$ cm^{-1} (there are several species present, even in frozen solution, due to slightly varying conformations, as found earlier even for CrR_4 complexes[25]). In parallel with analysis of current and previous EPR studies, we have also the electronic absorption spectra of CrL_4 complexes, using both classical LFT, as was done originally,[17,20,97] and using the latest ab initio methods. These methods each provide a general picture of the extensive Cr−L σ-bonding throughout and, in the $Cr(OR)_4$ complexes, relatively little π-bonding. The difference in electronic structure between $Cr(DTBMS)_4$ and the alkyl and alkoxide complexes with only light atoms may be due not only to the steric bulk of the DTBMS ligand, which imparts a tetragonal distortion slightly larger than in less encumbered complexes, but perhaps also to the effect of a heavier atom, Si as opposed

DOI: 10.1021/acs.inorgchem.8b03512
Inorg. Chem. 2019, 58, 4907−4920

to ligands containing only period 2 atoms. Nevertheless, the Cr^{IV} complexes with anionic O donor ligands are similar, not only to each other, but also to the tetraalkyl complexes in that π-donation by the O atoms is relatively insignificant. Amido complexes of formula $Cr(NR_2)_4$ are a different story. These were reported many years ago, but none was structurally characterized and no EPR spectra were recorded, despite attempts to do so. Our computational studies suggest that these simple amido complexes are also potentially very interesting, and it may be worth revisiting them synthetically to probe experimentally the possibility of their preference for a singlet ground state, as has been found experimentally for the Cr^{IV} tetraketimide complex, or at least their potentially large zfs, which may stem from the substantial and anisotropic π-donation by the amido ligands. The present experimental and theoretical results on Cr^{IV} in simple small molecules may also be helpful in providing a foundation for understanding (and distinguishing) multiple Cr sites in complicated, heterogeneous catalytic systems.

■ ASSOCIATED CONTENT

Supporting Information

The Supporting Information is available free of charge on the ACS Publications website at DOI: 10.1021/acs.inorgchem.8b03512.

Extended discussion of EPR spectra, of LFT, and of QCT as applied to CrL_4 complexes; LFT and QCT output tables; QTAIM figures; and calculated vibrational and electronic absorption figures (PDF)

■ AUTHOR INFORMATION

Corresponding Author

*E-mail: jtelser@roosevelt.edu.

ORCID

Lukas Bucinsky: 0000-0002-0190-3231
David C. Powers: 0000-0003-3717-2001
J. Krzystek: 0000-0001-6088-1936
Daniel G. Nocera: 0000-0001-5055-320X
Joshua Telser: 0000-0003-3307-2556

Notes

The authors declare no competing financial interest.

■ ACKNOWLEDGMENTS

This work was supported by NSF grant CHE-1464232 (to D.G.N.) and by grant A-1907 from the Welch Foundation (to D.C.P.). The HFEPR studies were supported by the NHMFL, which is funded by the NSF (Cooperative Agreement DMR 1157490) and the State of Florida. The computational studies were supported by the Slovak Grant Agency VEGA under contracts 1/0598/16 and 1/0466/18, and by the Slovak Science and Technology Assistance Agency APVV under contracts APVV-15-0079 and APVV-15-0053. We thank the HPC center at the Slovak University of Technology in Bratislava, which is a part of the Slovak Infrastructure of High Performance Computing (SIVVP Project ITMS 26230120002, funded by the European Region Development Funds) for computing facilities. L.B. and M.B. thank the Ministry of Education, Science, Research and Sport of the Slovak Republic for funding within the scheme "Excellent research teams". We thank Prof. Dr. Sebastian Riedel, Freie Universität Berlin, for very helpful discussions about CrF_4. Dr. Andrew Ozarowski, NHMFL, is acknowledged for his EPR simulation and fitting software SPIN.

■ REFERENCES

(1) Fong, A.; Vandervelden, C.; Scott, S. L.; Peters, B. Computational Support for Phillips Catalyst Initiation via Cr−C Bond Homolysis in a Chromacyclopentane Site. *ACS Catal.* **2018**, *8*, 1728−1733.

(2) Delley, M. F.; Lapadula, G.; Núñez-Zarur, F.; Comas-Vives, A.; Kalendra, V.; Jeschke, G.; Baabe, D.; Walter, M. D.; Rossini, A. J.; Lesage, A.; Emsley, L.; Maury, O.; Copéret, C. Local Structures and Heterogeneity of Silica-Supported M(III) Sites Evidenced by EPR, IR, NMR, and Luminescence Spectroscopies. *J. Am. Chem. Soc.* **2017**, *139*, 8855−8867.

(3) Barzan, C.; Piovano, A.; Braglia, L.; Martino, G. A.; Lamberti, C.; Bordiga, S.; Groppo, E. Ligands Make the Difference! Molecular Insights into Cr^{VI}/SiO_2 Phillips Catalyst during Ethylene Polymerization. *J. Am. Chem. Soc.* **2017**, *139*, 17064−17073.

(4) Brown, C.; Lita, A.; Tao, Y.; Peek, N.; Crosswhite, M.; Mileham, M.; Krzystek, J.; Achey, R.; Fu, R.; Bindra, J. K.; Polinski, M.; Wang, Y.; van de Burgt, L. J.; Jeffcoat, D.; Profeta, S.; Stiegman, A. E.; Scott, S. L. Mechanism of Initiation in the Phillips Ethylene Polymerization Catalyst: Ethylene Activation by Cr(II) and the Structure of the Resulting Active Site. *ACS Catal.* **2017**, *7*, 7442−7455.

(5) Brown, C.; Krzystek, J.; Achey, R.; Lita, A.; Fu, R.; Meulenberg, R. W.; Polinski, M.; Peek, N.; Wang, Y.; van de Burgt, L. J.; Profeta, S.; Stiegman, A. E.; Scott, S. L. Mechanism of Initiation in the Phillips Ethylene Polymerization Catalyst: Redox Processes Leading to the Active Site. *ACS Catal.* **2015**, *5*, 5574−5583.

(6) Delley, M. F.; Núñez-Zarur, F.; Conley, M. P.; Comas-Vives, A.; Siddiqi, G.; Norsic, S.; Monteil, V.; Safonova, O. V.; Copéret, C. Proton transfers are key elementary steps in ethylene polymerization on isolated chromium(III) silicates. *Proc. Natl. Acad. Sci. U. S. A.* **2014**, *111*, 11624−11629.

(7) Peters, B.; Scott, S. L.; Fong, A.; Wang, Y.; Stiegman, A. E. Reexamining the evidence for proton transfers in ethylene polymerization. *Proc. Natl. Acad. Sci. U. S. A.* **2015**, *112*, E4160.

(8) Delley, M. F.; Nuñez-Zarur, F.; Conley, M. P.; Comas-Vives, A.; Siddiqi, G.; Norsic, S.; Monteil, V.; Safonova, O. V.; Copéret, C. Reply to Peters et al.: Proton transfers are plausible initiation and termination steps on Cr(III) sites in ethylene polymerization. *Proc. Natl. Acad. Sci. U. S. A.* **2015**, *112*, E4162−E4163.

(9) Schrock, R. R.; Parshall, G. W. s-Alkyl and -Aryl Complexes of the Group 4−7 Transition Metals. *Chem. Rev.* **1976**, *76*, 243−268.

(10) Theopold, K. H. Homogeneous Chromium Catalysts for Olefin Polymerization. *Eur. J. Inorg. Chem.* **1998**, *1998*, 15−24.

(11) Amor Nait Ajjou, J.; Scott, S. L.; Paquet, V. Synthesis and Characterization of Silica-Stabilized Chromium(IV) Alkylidene Complexes. *J. Am. Chem. Soc.* **1998**, *120*, 415−416.

(12) Fujdala, K. L.; Tilley, T. D. Thermolytic Transformation of Tris(alkoxy)siloxychromium(IV) Single-Source Molecular Precursors to Catalytic Chromia−Silica Materials. *Chem. Mater.* **2001**, *13*, 1817−1827.

(13) Conley, M. P.; Delley, M. F.; Siddiqi, G.; Lapadula, G.; Norsic, S.; Monteil, V.; Safonova, O. V.; Copéret, C. Polymerization of Ethylene by Silica-Supported Dinuclear Cr^{III} Sites through an Initiation Step Involving C-H Bond Activation. *Angew. Chem., Int. Ed.* **2014**, *53*, 1872−1876.

(14) Mandal, D.; Mallick, D.; Shaik, S. Kinetic Isotope Effect Determination Probes the Spin of the Transition State, Its Stereochemistry, and Its Ligand Sphere in Hydrogen Abstraction Reactions of Oxoiron(IV) Complexes. *Acc. Chem. Res.* **2018**, *51*, 107−117.

(15) Holland, P. L. Distinctive Reaction Pathways at Base Metals in High-Spin Organometallic Catalysts. *Acc. Chem. Res.* **2015**, *48*, 1696−1702.

(16) Mowat, W.; Shortland, A.; Yagupsky, G.; Hill, N. J.; Yagupsky, M.; Wilkinson, G. Elimination stabilized alkyls. Part I. Chromium,

DOI: 10.1021/acs.inorgchem.8b03512
Inorg. Chem. 2019, 58, 4907−4920

molybdenum, tungsten, and vanadium. *J. Chem. Soc., Dalton Trans.* **1972**, 533−542.
(17) Mowat, W.; Shortland, A. J.; Hill, N. J.; Wilkinson, G. Elimination stabilized alkyls. Part II. Neopentyl and related alkyls of chromium(IV). *J. Chem. Soc., Dalton Trans.* **1973**, 770−778.
(18) Bochmann, M.; Wilkinson, G.; Young, G. B.; Hursthouse, M. B.; Malik, K. M. A. Synthesis and properties of bis(*t*-butyl)methoxides of chromium(III,IV), manganese(II), iron(III), cobalt(II), and copper(I). The crystal and molecular structures of lithium tetrakis-[bis(t-butyl)methoxo]chromate(III)-tetrahydrofuran (1/1), tetrakis-[bis(*t*-butyl)methoxo]chromium(IV), and lithium tetrakis[bis(*t*-butyl)methoxo]ferrate(III)-bis(*t*-butyl)-methanol (1/1). *J. Chem. Soc., Dalton Trans.* **1980**, 1863−1871.
(19) Stavropoulos, P.; Savage, P. D.; Tooze, R. P.; Wilkinson, G.; Hussain, B.; Motevalli, M.; Hursthouse, M. B. The synthesis and X-ray crystal structures of homoleptic tetrahedral aryls of osmium(IV) and of cyclohexyls of ruthenium(IV), osmium(IV), and chromium-(IV). *J. Chem. Soc., Dalton Trans.* **1987**, 557−562.
(20) Basi, J. S.; Bradley, D. C.; Chisholm, M. H. Covalent compounds of quadrivalent transition metals. Part III. Chromium(IV) dialkylamides. *J. Chem. Soc. A* **1971**, 1433−1436.
(21) Alyea, E. C.; Basi, J. S.; Bradley, D. C.; Chisholm, M. H. Covalent compounds of quadrivalent transition metals. Part II. Chromium(IV) tertiary alkoxides and triethylsilyloxide. *J. Chem. Soc. A* **1971**, 772−776.
(22) Bower, B. K.; Tennent, H. G. Transition metal bicyclo[2.2.1]-hept-1-yls. *J. Am. Chem. Soc.* **1972**, *94*, 2512−2514.
(23) Kruse, W. Preparation of peralkylchromium(IV) compounds. *J. Organomet. Chem.* **1972**, *42*, C39−C42.
(24) Ward, G. A.; Kruse, W.; Bower, B. K.; Chien, J. C. W. EPR spectra of chromium(IV) in tetrakis-alkyl chromium compounds. *J. Organomet. Chem.* **1972**, *42*, C43−C46.
(25) Ward, G. A.; Bower, B. K.; Findlay, M.; Chien, J. C. W. Electron paramagnetic resonance of tetrakis(1-norbonyl)chromium. *Inorg. Chem.* **1974**, *13*, 614−617.
(26) Alonso, P. J.; Forniés, J.; García-Monforte, M. A.; Martín, A.; Menjón, B.; Rillo, C. Synthesis and characterization of new paramagnetic tetraaryl derivatives of chromium and molybdenum. *J. Organomet. Chem.* **2007**, *692*, 3236−3247.
(27) Alonso, P. J.; Forniés, J.; García-Monforte, M. A.; Martín, A.; Menjón, B.; Rillo, C. A New Series of Homoleptic, Paramagnetic Organochromium Derivatives: Synthesis, Characterization, and Study of Their Magnetic Properties. *Chem. - Eur. J.* **2002**, *8*, 4056−4065.
(28) Groysman, S.; Villagrán, D.; Nocera, D. G. Pseudotetrahedral d^0, d^1, and d^2 Metal−Oxo Cores within a Tris(alkoxide) Platform. *Inorg. Chem.* **2010**, *49*, 10759−10761.
(29) Chadeayne, A. R.; Wolczanski, P. T.; Lobkovsky, E. B. The Course of $(R_2R'SiO)_3TaCl_2$ (R = ^{t}Bu, R' = H, Me, Ph, ^{t}Bu (silox); R = iPr, R' = ^{t}Bu, ^{i}Pr) Reduction Is Dependent on Siloxide Size. *Inorg. Chem.* **2004**, *43*, 3421−3432.
(30) Marshak, M. P.; Nocera, D. G. Chromium(IV) Siloxide. *Inorg. Chem.* **2013**, *52*, 1173−1175.
(31) Soriaga, R. A. D.; Nguyen, J. M.; Albright, T. A.; Hoffman, D. M. Diamagnetic Group 6 Tetrakis(di-*tert*-butylketimido)metal(IV) Complexes. *J. Am. Chem. Soc.* **2010**, *132*, 18014−18016.
(32) Johnson, D. A.; Nelson, P. G. Factors Determining the Ligand Field Stabilization Energies of the Hexaaqua 2+ Complexes of the First Transition Series and the Irving-Williams Order. *Inorg. Chem.* **1995**, *34*, 5666−5671.
(33) Johnson, D. A.; Nelson, P. G. Ligand Field Stabilization Energies of the Hexaaqua 3+ Complexes of the First Transition Series. *Inorg. Chem.* **1999**, *38*, 4949−4955.
(34) Wolczanski, P. T. Chemistry of electrophilic metal centres coordinated by silox (^{t}Bu$_3$SiO), tritox (^{t}Bu$_3$CO) and related binfunctional ligands. *Polyhedron* **1995**, *14*, 3335−3362.
(35) Bucinsky, L.; Breza, M.; Lee, W.-T.; Hickey, A. K.; Dickie, D. A.; Nieto, I.; DeGayner, J. A.; Harris, T. D.; Meyer, K.; Krzystek, J.; Ozarowski, A.; Nehrkorn, J.; Schnegg, A.; Holldack, K.; Herber, R. H.; Telser, J.; Smith, J. M. Spectroscopic and Computational Studies of Spin States of Iron(IV) Nitrido and Imido Complexes. *Inorg. Chem.* **2017**, *56*, 4751−4768.
(36) Bucinsky, L.; Rohde, G. T.; Que, L., Jr.; Ozarowski, A.; Krzystek, J.; Breza, M.; Telser, J. HFEPR and Computational Studies on the Electronic Structure of a High-Spin Oxidoiron(IV) Complex in Solution. *Inorg. Chem.* **2016**, *55*, 3933−3945.
(37) Krzystek, J.; England, J.; Ray, K.; Ozarowski, A.; Smirnov, D.; Que, L., Jr.; Telser, J. Determination by High-Frequency and -Field EPR of Zero-Field Splitting in Iron(IV) Oxo Complexes: Implications for Intermediates in Nonheme Iron Enzymes. *Inorg. Chem.* **2008**, *47*, 3483−3485.
(38) Damon, P. L.; Liss, C. J.; Lewis, R. A.; Morochnik, S.; Szpunar, D. E.; Telser, J.; Hayton, T. W. Quantifying the Electron Donor and Acceptor Abilities of the Ketimide Ligands in $M(N{=}C^tBu_2)_4$ (M = V, Nb, Ta). *Inorg. Chem.* **2015**, *54*, 10081−10095.
(39) Krzystek, J.; Ozarowski, A.; Telser, J. Multi-frequency, high-field EPR as a powerful tool to accurately determine zero-field splitting in high-spin transition metal coordination complexes. *Coord. Chem. Rev.* **2006**, *250*, 2308−2324.
(40) Telser, J.; Krzystek, J.; Ozarowski, A. High-frequency and high-field electron paramagnetic resonance (HFEPR): a new spectroscopic tool for bioinorganic chemistry. *JBIC, J. Biol. Inorg. Chem.* **2014**, *19*, 297−318.
(41) Bougon, R.; Wilson, W. W.; Christe, K. O. Synthesis and characterization of tetrafluoroammonium hexafluorochromate and reaction chemistry of chromium pentafluoride. *Inorg. Chem.* **1985**, *24*, 2286−2292.
(42) Wartenberg, H. Über höhere Chromfluoride (CrF_4, CrF_5 und CrO_2F_2). *Z. Anorg. Allg. Chem.* **1941**, *247*, 135−146.
(43) Osin, S. B.; Davliasthin, D. I.; Ogden, J. S. A study of the reactions of fluorine with chromium and iron at high temperatures by matrix isolation IR spectroscopy. *J. Fluorine Chem.* **1996**, *76*, 187−192.
(44) Schlöder, T.; Brosi, F.; Freyh, B. J.; Vent-Schmidt, T.; Riedel, S. New Evidence in an Old Case: The Question of Chromium Hexafluoride Reinvestigated. *Inorg. Chem.* **2014**, *53*, 5820−5829.
(45) Hedberg, L.; Hedberg, K.; Gard, G. L.; Udeaja, J. O.; et al. Molecular Structure of Chromium Tetrafluoride in the Gas Phase. *Acta Chem. Scand.* **1988**, *42a*, 318−323.
(46) Jacobs, J.; Mueller, H. S. P.; Willner, H.; Jacob, E.; Bürger, H. Vibrational and electronic spectra of molecular chromium tetrafluoride, CrF_4, and chromium pentafluoride, CrF_5. Comments on the existence of chromium hexafluoride, CrF_6. *Inorg. Chem.* **1992**, *31*, 5357−5363.
(47) Wasserman, E.; Snyder, L. C.; Yager, W. A. ESR of the Triplet States of Randomly Oriented Molecules. *J. Chem. Phys.* **1964**, *41*, 1763−1772.
(48) Weil, J. A.; Bolton, J. R. *Electron Paramagnetic Resonance: Elementary Theory and Practical Applications*, 2nd ed.; John Wiley & Sons, Inc.: Hoboken, NJ, 2007.
(49) Klinker, E. J.; Shaik, S.; Hirao, H.; Que, L., Jr. A Two-State Reactivity Model Explains Unusual Kinetic Isotope Effect Patterns in C-H Bond Cleavage by Nonheme Oxoiron(IV) Complexes. *Angew. Chem., Int. Ed.* **2009**, *48*, 1291−1295.
(50) Hassan, A. K.; Pardi, L. A.; Krzystek, J.; Sienkiewicz, A.; Goy, P.; Rohrer, M.; Brunel, L.-C. Ultrawide band multifrequency high-field EMR technique: a methodology for increasing spectroscopic information. *J. Magn. Reson.* **2000**, *142*, 300−312.
(51) Bendix, J. Ligfield. In *Comprehensive Coordination Chemistry II, Vol. 2: Fundamentals: Physical Methods, Theoretical Analysis, and Case Studies*; Lever, A. B. P., Ed.; Elsevier: Amsterdam, 2003; Vol. 2, pp 673−676.
(52) Brorson, M.; Schäffer, C. E., Orthonormal interelectronic repulsion operators in the parametrical d^q model. Application of the model to gaseous ions. *Inorg. Chem.* **1988**, *27*, 2522−2530.
(53) Bendix, J.; Brorson, M.; Schäffer, C. E. Accurate empirical spin orbit coupling parameters z_{nd} for gaseous nd^q transition metal ions. The parametrical multiplet term model. *Inorg. Chem.* **1993**, *32*, 2838−2849.

DOI: 10.1021/acs.inorgchem.8b03512
Inorg. Chem. 2019, 58, 4907−4920

(54) Frisch, M. J.; Trucks, G. W.; Schlegel, H. B.; Scuseria, G. E.; Robb, M. A.; Cheeseman, J. R.; Scalmani, G.; Barone, V.; Mennucci, B.; Petersson, G. A.; Nakatsuji, H.; Caricato, M.; Li, X.; Hratchian, H. P.; Izmaylov, A. F.; Bloino, J.; Zheng, G.; Sonnenberg, J. L.; Hada, M.; Ehara, M.; Toyota, K.; Fukuda, R.; Hasegawa, J.; Ishida, M.; Nakajima, T.; Honda, Y.; Kitao, O.; Nakai, H.; Vreven, T.; Montgomery, J. A., Jr.; Peralta, J. E.; Ogliaro, F.; Bearpark, M.; Heyd, J. J.; Brothers, E.; Kudin, K. N.; Staroverov, V. N.; Kobayashi, R.; Normand, J.; Raghavachari, K.; Rendell, A.; Burant, J. C.; Iyengar, S. S.; Tomasi, J.; Cossi, M.; Rega, N.; Millam, J. M.; Klene, M.; Knox, J. E.; Cross, J. B.; Bakken, V.; Adamo, C.; Jaramillo, J.; Gomperts, R.; Stratmann, R. E.; Yazyev, O.; Austin, A. J.; Cammi, R.; Pomelli, C.; Ochterski, J. W.; Martin, R. L.; Morokuma, K.; Zakrzewski, V. G.; Voth, G. A.; Salvador, P.; Dannenberg, J. J.; Dapprich, S.; Daniels, A. D.; Farkas, O.; Foresman, J. B.; Ortiz, J. V.; Cioslowski, J.; Fox, D. J. *Gaussian 09, Revision D.01*; Gaussian, Inc.: Wallingford CT, 2009.
(55) Lee, C.; Yang, W.; Parr, R. G. Development of the Colle-Salvetti correlation-energy formula into a functional of the electron density. *Phys. Rev. B: Condens. Matter Mater. Phys.* **1988**, *37*, 785−789.
(56) Becke, A. D. Density-functional Thermochemistry. III. The Role of Exact Exchange. *J. Chem. Phys.* **1993**, *98*, 5648−5652.
(57) Stephens, P. J.; Devlin, F. J.; Chabalowski, C. F.; Frisch, M. J. Ab Initio Calculation of Vibrational Absorption and Circular Dichroism Spectra Using Density Functional Force Fields. *J. Phys. Chem.* **1994**, *98*, 11623−11627.
(58) Vosko, S. H.; Wilk, L.; Nusair, M. Accurate spin-dependent electron liquid correlation energies for local spin density calculations: a critical analysis. *Can. J. Phys.* **1980**, *58*, 1200−1211.
(59) Krishnan, R.; Binkley, J. S.; Seeger, R.; Pople, J. A. Self-consistent molecular orbital methods. XX. A basis set for correlated wave functions. *J. Chem. Phys.* **1980**, *72*, 650−654.
(60) McLean, A. D.; Chandler, G. S. Contracted Gaussian basis sets for molecular calculations. I. Second row atoms, Z = 11−18. *J. Chem. Phys.* **1980**, *72*, 5639−5648.
(61) Wachters, A. J. H. Gaussian Basis Set for Molecular Wavefunctions Containing Third-Row Atoms. *J. Chem. Phys.* **1970**, *52*, 1033−1036.
(62) Ugliengo, P. *MOLDRAW: A Program to Display and Manipulate Molecular and Crystal Structures*; Torino, Italy, 2006.
(63) Bachler, V.; Olbrich, G.; Neese, F.; Wieghardt, K. Theoretical Evidence for the Singlet Diradical Character of Square Planar Nickel Complexes Containing Two *o*-Semiquinonato Type Ligands. *Inorg. Chem.* **2002**, *41*, 4179−4193.
(64) Herebian, D.; Wieghardt, K. E.; Neese, F. Analysis and Interpretation of Metal-Radical Coupling in a Series of Square Planar Nickel Complexes: Correlated Ab Initio and Density Functional Investigation of $[Ni(L^{ISQ})_2]$ (L^{ISQ}=3,5-di-*tert*-butyl-*o*-diiminobenzosemiquinonate(1-)). *J. Am. Chem. Soc.* **2003**, *125*, 10997−11005.
(65) Blanchard, S.; Neese, F.; Bothe, E.; Bill, E.; Weyhermüller, T.; Wieghardt, K. Square Planar vs Tetrahedral Coordination in Diamagnetic Complexes of Nickel(II) Containing Two Bidentate π-Radical Monoanions. *Inorg. Chem.* **2005**, *44*, 3636−3656.
(66) Chłopek, K.; Bothe, E.; Neese, F.; Weyhermüller, T.; Wieghardt, K. Molecular and Electronic Structures of Tetrahedral Complexes of Nickel and Cobalt Containing *N,N'*-Disubstituted, Bulky o-Diiminobenzosemiquinonate(1−) π-Radical Ligands. *Inorg. Chem.* **2006**, *45*, 6298−6307.
(67) Chłopek, K.; Muresan, N.; Neese, F.; Wieghardt, K. Electronic Structures of Five-Coordinate Complexes of Iron Containing Zero, One, or Two π-Radical Ligands: A Broken-Symmetry Density Functional Theoretical Study. *Chem. - Eur. J.* **2007**, *13*, 8390−8403.
(68) Yamaguchi, K.; Tsunekawa, T.; Toyoda, Y.; Fueno, T. Ab initio molecular orbital calculations of effective exchange integrals between transition metal ions. *Chem. Phys. Lett.* **1988**, *143*, 371−376.
(69) Neese, F. Importance of Direct Spin−Spin Coupling and Spin-Flip Excitations for the Zero-Field Splittings of Transition Metal Complexes: A Case Study. *J. Am. Chem. Soc.* **2006**, *128*, 10213−10222.
(70) Neese, F. Prediction of electron paramagnetic resonance g values using coupled perturbed Hartree−Fock and Kohn−Sham theory. *J. Chem. Phys.* **2001**, *115*, 11080−11096.
(71) Sandhoefer, B.; Neese, F. One-electron contributions to the g-tensor for second-order Douglas−Kroll−Hess theory. *J. Chem. Phys.* **2012**, *137*, No. 094102.
(72) Neese, F. *ORCA—An ab Initio, Density Functional and Semiempirical Program Package, 4.0.1.2*; Max Planck Institut für Kohlenforschung: Mülheim an der Ruhr, Germany, 2018.
(73) Neese, F. The ORCA program system. *Wiley Interdisciplinary Reviews: Computational Molecular Science* **2012**, *2*, 73−78.
(74) Schäfer, A.; Horn, H.; Ahlrichs, R. Fully optimized contracted Gaussian basis sets for atoms Li to Kr. *J. Chem. Phys.* **1992**, *97*, 2571−2577.
(75) Duboc, C.; Ganyushin, D.; Sivalingam, K.; Collomb, M.-N.; Neese, F. Systematic Theoretical Study of the Zero-Field Splitting in Coordination Complexes of Mn(III). Density Functional Theory versus Multireference Wave Function Approaches. *J. Phys. Chem. A* **2010**, *114*, 10750−10758.
(76) Zein, S.; Neese, F. Ab Initio and Coupled-Perturbed Density Functional Theory Estimation of Zero-Field Splittings in Mn^{II} Transition Metal Complexes. *J. Phys. Chem. A* **2008**, *112*, 7976−7983.
(77) Romain, S.; Duboc, C.; Neese, F.; Rivière, E.; Hanton, L. R.; Blackman, A. G.; Philouze, C.; Leprêtre, J.-C.; Deronzier, A.; Collomb, M.-N. An Unusual Stable Mononuclear Mn^{III} Bis-terpyridine Complex Exhibiting Jahn−Teller Compression: Electrochemical Synthesis, Physical Characterisation and Theoretical Study. *Chem. - Eur. J.* **2009**, *15*, 980−988.
(78) Angeli, C.; Cimiraglia, R.; Evangelisti, S.; Leininger, T.; Malrieu, J.-P. Introduction of n-electron valence states for multi-reference perturbation theory. *J. Chem. Phys.* **2001**, *114*, 10252−10264.
(79) Angeli, C.; Cimiraglia, R.; Malrieu, J.-P. N-electron valence state perturbation theory: a fast implementation of the strongly contracted variant. *Chem. Phys. Lett.* **2001**, *350*, 297−305.
(80) Angeli, C.; Evangelisti, S.; Cimiraglia, R.; Maynau, D. A novel perturbation-based complete active space−self-consistent-field algorithm: Application to the direct calculation of localized orbitals. *J. Chem. Phys.* **2002**, *117*, 10525−10533.
(81) Havenith, R. W. A.; Taylor, P. R.; Angeli, C.; Cimiraglia, R.; Ruud, K. Calibration of the n-electron valence state perturbation theory approach. *J. Chem. Phys.* **2004**, *120*, 4619−4625.
(82) Pipek, J.; Mezey, P. G. A fast intrinsic localization procedure applicable for *ab initio* and semiempirical linear combination of atomic orbital wave functions. *J. Chem. Phys.* **1989**, *90*, 4916−4926.
(83) Bader, R. F. W. *Atoms in Molecules: A Quantum Theory*; Clarendon Press: Oxford, UK, 1994.
(84) Keith, T. A. *AIMAll, 17.11.14*; TK Gristmill Software: Overland Park, KS, 2017.
(85) Gilbert, A. *IQmol, 2.8.0*; 2018.
(86) Llunell, M.; Casanova, D.; Cirera, J.; Alemany, P.; Alvarez, S. *SHAPE: Program for the Stereochemical Analysis of Molecular Fragments by Means of Continuous Shape Measures and Associated Tools, 2.1*; Barcelona, Catalonia, Spain, 2013.
(87) Falceto, A.; Casanova, D.; Alemany, P.; Alvarez, S. Pseudo-symmetry Analysis of the d-block Molecular Orbitals in Four-Coordinate Complexes. *Inorg. Chem.* **2013**, *52*, 6510−6519.
(88) Charron, G.; Bellot, F.; Cisnetti, F.; Pelosi, G.; Rebilly, J.-N.; Rivière, E.; Barra, A.-L.; Mallah, T.; Policar, C. Glycoligands Tuning the Magnetic Anisotropy of Ni^{II} Complexes. *Chem. - Eur. J.* **2007**, *13*, 2774−2782.
(89) Wojciechowska, A.; Daszkiewicz, M.; Staszak, Z.; Trusz-Zdybek, A.; Bieńko, A.; Ozarowski, A. Synthesis, Crystal Structure, Spectroscopic, Magnetic, Theoretical and Micro-biological Studies of a Nickel(II) Complex of L-Tyrosine and Imidazole, $[Ni(Im)_2(L\text{-}tyr)_2]\cdot 4H_2O$. *Inorg. Chem.* **2011**, *50*, 11532−11542.
(90) Dobrzyńska, D.; Jerzykiewicz, L. B.; Duczmal, M.; Wojciechowska, A.; Jabłońska, K.; Palus, J.; Ozarowski, A. Structural, Spectroscopic, and Magnetic Study of Bis(9,10-dihydro-9-oxo-10-

DOI: 10.1021/acs.inorgchem.8b03512
Inorg. Chem. 2019, 58, 4907−4920

acridineacetate)bis(imidazole)bis(methanol) Nickel(II). *Inorg. Chem.* **2006**, *45*, 10479−10486.
(91) Wojciechowska, A.; Gagor, A.; Duczmal, M.; Staszak, Z.; Ozarowski, A. L-Tyrosinatonickel(II) Complex: Synthesis and Structural, Spectroscopic, Magnetic, and Biological Properties of $2\{[Ni(l\text{-}Tyr)_2(bpy)]\}\cdot 3H_2O\cdot CH_3OH$. *Inorg. Chem.* **2013**, *52*, 4360−4371.
(92) Pladzyk, A.; Ozarowski, A.; Ponikiewski, Ł. Crystal and electronic structures of Ni(II) silanethiolates containing flexible diamine ligands. *Inorg. Chim. Acta* **2016**, *440*, 84−93.
(93) Jiang, P.; Li, J.; Ozarowski, A.; Sleight, A. W.; Subramanian, M. A. Intense Turquoise and Green Colors in Brownmillerite-Type Oxides Based on Mn^{5+} in $Ba_2In_{2-x}Mn_xO_{5+x}$. *Inorg. Chem.* **2013**, *52*, 1349−1357.
(94) Krzystek, J.; Ozarowski, A.; Zvyagin, S. A.; Telser, J. High Spin Co(I): High-Frequency and -Field EPR Spectroscopy of $CoX(PPh_3)_3$ (X = Cl, Br). *Inorg. Chem.* **2012**, *51*, 4954−4964.
(95) Estimated by inspection of Figure 2 in Mowat et al.[17]
(96) Cirera, J.; Alemany, P.; Alvarez, S. Mapping the Stereochemistry and Symmetry of Tetracoordinate Transition-Metal Complexes. *Chem. - Eur. J.* **2004**, *10*, 190−207.
(97) Abrahamson, H. B.; Brandenburg, K. L.; Lucero, B.; Martin, M. E.; Dennis, E. Spectroscopy and photochemistry of the tetranorbornyl complexes of titanium and chromium. *Organometallics* **1984**, *3*, 1379−1386.
(98) An alternate analysis, which is based on an assumption as to the $^3A_2 \rightarrow {}^3T_1(P)$ transition, is discussed in SI (see Table S3, Figure S1).
(99) Schäffer, C. E. A Perturbation Representation of Weak Covalent Bonding. *Struct. Bonding (Berlin)* **1968**, *5*, 68−95.
(100) Abragam, A.; Bleaney, B. *Electron Paramagnetic Resonance of Transition Ions (Oxford Classic Texts in the Physical Sciences)*; Oxford University Press: Oxford, UK, 2012.
(101) This equation is equivalent to that given in Abragam and Bleaney,[97] Table 7.7: $g = g_e - \frac{8\lambda'}{\Delta}$ where $\Delta \equiv 10Dq$ and $g_e \approx 2$. It is applicable to tetrahedral d^2, octahedral d^8, tetrahedral d^7, and octahedral d^3 electronic configurations. Mowat et al.[17] provide equations for $g_\parallel$ and $g_\perp$, using the respective energies of the $^3B_2$ and ^3E excited states derived from $^3T_2(F)$, but since our values for $g_\parallel$ are only estimates, this approach is not worthwhile.
(102) They used $\lambda_0 = 170\ cm^{-1}$ and $10Dq = 10\,000\ cm^{-1}$. The above LFT analysis suggests that $10Dq \sim 9300\ cm^{-1}$, which, with the current value, $\lambda_0 = 160\ cm^{-1}$, gives $k = 0.544$.
(103) Using the AOM, where $10Dq = \left(\frac{4}{3}\right)\varepsilon_\sigma - \left(\frac{8}{9}\right)\varepsilon_{\pi-s}$,[104] then the respective k values are 0.82 (A) and 0.70 (B and C), which are essentially the same as in the tetrahedral model.
(104) Miessler, G. L.; Fischer, P. J.; Tarr, D. A. *Inorganic Chemistry*; Pearson: Upper Saddle River, NJ, 2014.
(105) A typo in the original equation has been corrected, and we use an isotropic SOC constant; we also add the contribution from the second $^1T_2$ term, which arises largely from free-ion ^1G (see Figure 5).
(106) Note that the ketimide ligand can also be a π-acceptor, via $\varepsilon_{\pi-s}$, which is unreasonable in the present complexes that have a ligand with only saturated (alkyl) substituents.
(107) While the lack of exact (Hartree−Fock) exchange in the case of BLYP leads to the preference of the low-spin state of $Cr(NMe_2)_4$, the high-spin state is preferred with exact exchange taken into account in the B3LYP and CASSCF calculations. Remarkably, with the inclusion of dynamic electron correlation, the lowest singlet root becomes the energetically preferred configuration in the NEVPT2 calculation (see Tables S10 and S11) keeping the $d_{x^2-y^2}$ closed-shell character
(108) Steric repulsion among the bulky groups in $Cr(NMeCH^tBu_2)_4$ may lead to larger Cr−N bond distances and structural differences relative to $Cr(NMe_2)_4$, which in turn causes reordering or shifting of the Cr^{IV} 3d orbitals. This leads to a preference of triplet over singlet in $Cr(NMeCH^tBu_2)_4$ even at the BLYP level of theory, as suggested by the B3LYP $(G_S - G_T)_{298}$ values as well (see Table 3).
(109) For C^+ (C II in spectroscopic notation, $2s^22p^1$), $\zeta_{2p} = 42.28\ cm^{-1}$, while for Si^+ (Si II, $3s^23p^1$), $\zeta_{3p} = 191.49\ cm^{-1}$, 4.5× larger. For C^0 (C I, $2s^22p^2$), $\zeta \approx 30\ cm^{-1}$, while for Si^0 (Si I, $3s^23p^2$), $\zeta \approx 150\ cm^{-1}$.[110]
(110) Ralchenko, Y.; Kramida, A. E.; Reader, J.; NIST ASD Team. *NIST Atomic Spectra Database (ver. 5.5.6)*; National Institute of Standards and Technology: Gaithersburg, MD, 2018.
(111) Accounting for dynamic electron correlation (NEVPT2) leads to a considerable improvement of zfs parameters in the cases of both $Cr(NMeCH^tBu_2)_4$ and $Cr(NMe_2)_4$ with C_2 symmetry, and these agree well with the zfs parameters calculated from BLYP.
(112) To put the CASSCF results for the amido complexes under a further spotlight, we have performed state averaged CASSCF calculations using the 15 singlet states as the reference (taking into account that the singlet state could be preferred) and keeping the 10 triplet state roots still present. This singlet-state-based CASSCF calculation leads to a considerable improvement of the D value magnitudes with respect to NEVPT2 triplet-state-based results, see Table S14 (Supporting Information).
(113) For example, at 9.5 GHz, a resonance might be observed at a field inaccessible to conventional X-band EPR spectrometers, namely, ∼1.0 T.
(114) Calculated $D = +0.43\ cm^{-1}$ versus experimental $+0.43\ cm^{-1}$ for species C, $+0.56\ cm^{-1}$ for B, and $+0.76\ cm^{-1}$ for A. The slight changes in morphology/disorder that might lead to these are not known.
(115) Treating the alkoxide and siloxide complexes together, we find that the results for $Cr(DTBMS)_4$ fit better with experiment when considering the experimental geometry rather than the optimized one (see Table 4). In particular, the CAS and $MRCI_{MIN}$ magnetic parameters are to be highlighted with respect to the experimentally determined values. On the other hand, the optimized structure of $Cr(DTBMS)_4$ yields an overestimated D value (by almost 2 times) at the CAS or $MRCI_{MIN}$ level, although the g values remain reasonable. This difficulty is reminiscent of the problems of applying LFT to calculating zfs for $Cr(DTBMS)_4$.
(116) Furthermore, the bulky DTBMS and/or $^-OSiMe(^tBu)_2$ ligand can be more sensitive to geometry optimization with respect to the orientation of the ligand itself and with respect to geometry of the coordination polyhedron compared to a crystal phase or frozen solution. Qualitatively, this sensitivity is also manifest in the multiple species found by HFEPR as well as the disorder in the crystal structure. Even though the differences are not dramatic, the four equal bonds in the optimized geometry of $Cr(DTBMS)_4$ (1.772 Å) are longer than those found in the crystal structure (1.764 Å; see Table S1). Although the asymmetry in the experimental geometry is small, this can make an important contribution to the final sign and/or magnitude of the D parameter of the complex.
(117) $Cr(OMe)_4$ in an ideal tetrahedral geometry with d(CrO) = 1.766 Å was distorted systematically to (i) C_{2v} geometry by maintaining the ideal tetrahedral ∠O−Cr−O = 109.47°, but shortening/elongating two Cr−O bond distances; (ii) C_{3v} geometry by maintaining the ideal tetrahedral ∠O−Cr−O, but shortening/elongating one Cr−O bond distance; and (iii) D_{2d} geometry by maintaining d(CrO) = 1.766 Å, but increasing a pair of ∠O−Cr−O that are related by the S_4 axis in D_{2d} symmetry. Each geometrical change was made in a stepwise fashion with the zfs calculated for each structure. For comparison, the same process was applied to CrF_4 with d(CrF) = 1.714 Å.
(118) Note that, for ideal C_{3v} and D_{2d} symmetry, the x and y directions are equivalent so $E = 0$; we ignore the calculated E value for C_{2v} for ease of comparison among the three cases.

DOI: 10.1021/acs.inorgchem.8b03512
Inorg. Chem. 2019, 58, 4907−4920